IEEE Access
Multidisciplinary | Rapid Review | Open Access Journal

Received June 1, 2017, accepted July 6, 2017, date of publication July 20, 2017, date of current version August 8, 2017.

Digital Object Identifier 10.1109/ACCESS.2017.2728372

RF Sensing Based Target Detector for Smart Sensing Within Internet of Things in Harsh Sensing Environments

SIVA KARTEEK BOLISETTI[1], (Student Member, IEEE), MOHAMMAD PATWARY[2], (Senior Member, IEEE), ABDEL-HAMID SOLIMAN[1], AND MOHAMED ABDEL-MAGUID[3], (Senior Member, IEEE)

[1]School of Creative Arts and Engineering, Staffordshire University, Stoke-on-Trent ST4 2DE, U.K.
[2]School of Computing and Digital Technology, Birmingham City University, Birmingham B5 5JU, U.K.
[3]Department of Science and Technology, University of Suffolk, Ipswich IP4 1QJ, U.K.

Corresponding author: Siva Karteek Bolisetti (bolisettisk@ieee.org)

ABSTRACT In this paper, we explore surveillance and target detection applications of Internet of Things (IoT) with radio detection as the primary means of sensing. The problem of surveillance and target detection has found its place in numerous civilian and military applications, and IoT is well suited to address this problem. Radio frequency (RF) sensing techniques are the next generation technologies, which offer distinct advantages over traditional means of sensing used for surveillance and target detection applications of IoT. However, RF sensing techniques have yet to be widely researched due to lack of transmission and computational resources within IoT. Recent advancements in sensing, computing, and communication technologies have made radio detection enabled sensing techniques available to IoT. However, extensive research is yet to be done in developing reliable and energy efficient target detection algorithms for resource constrained IoT. In this paper, we have proposed a multi-sensor RF sensing-based target detection architecture for IoT. The proposed target detection architecture is adaptable to interference, which is caused due to the co-existence of sensor nodes within IoT and adopts smart sensing strategies to reliably detect the presence of the targets. A waveform selection criterion has been proposed to identify the optimum choice of transmit waveforms within a given set of sensing conditions to optimize the target detection reliability and power consumption within the IoT. A dual-stage target detection strategy has been proposed to reduce the computational burden and increase the lifetime of the sensor nodes.

INDEX TERMS Energy efficiency, Internet of Things (IoT), multi-sensor, RF sensing, target detection.

I. INTRODUCTION

IoT consists of low cost, easy-to-use, easy-to-deploy network of active or passive sensor nodes, which are deployed within the sensing region. Depending on the nature of the sensing application, the sensor nodes can be deployed either randomly or in an organised fashion. Once deployed, the sensor nodes collect data, which can be used to perform tasks such as surveillance, remote monitoring, etc. The sensor nodes are equipped with one of more sensing devices with limited power, processing, and communication capabilities. Sensor nodes collectively monitor the sensing region and respond to the occurrence of unexpected events or relay the information to a centralised control centre. The control centre, which is usually equipped with additional power and processing resources, collects the data from all the sensor nodes and makes a decision regarding the occurrence of the event.

In recent times, IoT [1], [2] have experienced increased attention in civilian, industrial, and military applications. Due to low-cost and cooperative nature of sensor nodes, IoT is well suited for surveillance applications [3], [4]. Some of the surveillance applications of IoT include battlefield surveillance, remote monitoring in urban environments, intrusion detection, etc. Sensor nodes can be deployed in hazardous battlefield environments to monitor enemy activities while keeping the human operator at safety. Depending on the nature of the sensing application, the sensor nodes can either actively interact with the sensing environment or passively monitor the same. Jaigirdar *et al.* [5] have discussed the

introduction of active sensor nodes within the sensing region. While active sensor nodes allow aggressive sensing strategies to achieve increased reliability, the increased power consumption within resource limited sensor nodes must be taken into account while designing the network. Within the existing literature, to the best of author's knowledge, limited research has been done towards developing RF sensing based IoT.

For IoT deployed in harsh sensing environments, there is a need to develop robust target detectors, which provide reliable target detection rates while being computationally efficient. Most often within IoT, the sensor nodes are required to operate in harsh sensing environments in the presence of clutter and interfering signals. The sensor nodes while co-existing with the other sensor nodes are required to provide reliable target detection rates while using the limited available power and processing capabilities. Our proposed target detector is expected to give an energy efficient solution to the problem of target detection under these sensing conditions. To optimise the target detector, we divide the target detection procedure into initialisation and operational stages. Preliminary time-invariant estimations are performed in initialisation stage and the final decisions are made using the received signal samples obtained during the operational stage. Amount of data transfer between the sensor nodes and the control centre has a severe impact on the lifetime of sensor nodes. We proposed compressive sensing to reduce the transmissions costs. Finally, we propose a waveform selection strategy to optimise the reliability and energy efficiency of the target detector. The main contributions of this paper are as follows:

1) RF sensing based target detection architecture for surveillance applications of IoT has been proposed in this paper.
2) An optimised dual-stage target detection strategy has been proposed to improve the computational efficiency of the target detector.
3) To increase the lifetime of the sensor nodes we propose compressive sensing where the sensor nodes are only required to transmit reduced number of compressed received signal samples to the control centre.
4) We propose a waveform selection criterion to optimise the energy efficiency and target detection reliability of the sensor nodes within the IoT while co-existing with the other sensor nodes.

Rest of the paper is organised as follows: The existing literature related to our work is elaborated in Section II. Problem formulation for the proposed IoT and the expected received signal models are discussed in Section III. Inverse covariance estimation procedure for target detection is discussed in Section IV and elaborated in Appendix. In Section V we derive the test statistic for the proposed target detector. In Section VI we discuss the waveform selection criterion for co-existence of sensor nodes within IoT. Simulation results are discussed in Section VII followed by conclusion and future work in Section VIII.

II. RELATED WORK

Sensing the presence or absence of a target is one of the primary objectives of IoT for surveillance applications. Traditionally, IoT used infrared, magnetic, seismic, acoustics, optics, etc. as primary means of sensing. Intrusion detection for surveillance applications is a problem, which is well suited for IoT. However, RF sensing based target detection within IoT has not yet been widely researched. RF sensing involves transmitting RF signals into the sensing region and detecting reflected components of the transmitted signals to detect the presence of targets [6]–[8]. Some of the major advantages of using RF sensing are no line-of-sight requirement, ability to distinguish between targets and non-targets, ability to operate through obstacles, ability to estimate range and velocity of the targets, etc. Commercial widespread applications of RF sensing have not yet been possible due to limitations over power consumption and processing requirements. With the development of micropower impulse radios, RF sensing based IoT has become a possibility. Ultra-Wideband (UWB) technology was developed at Lawrence Livermore National Labs [9] which uses micropower impulses as against to conventional narrowband transmissions. Micropower impulses in UWB technology are transmitted for a short duration of time and hence contain little energy. Ditzel and Elferink [7] designed a low-power RF sensing platform based on UWB technology and investigated the power budget and energy breakdown for the sensor node. These sensor nodes are compact and low powered which makes them ideal for IoT. Subsequent developments [10] resulted in designing RF sensing based autonomous network of sensor nodes with significant improvements in sensing range and power consumption. An autonomous sensor network is expected to have the ability to gather the sensing data and use intelligent design framework to support autonomous decision-making capabilities to detect and track targets within the sensing range.

Power consumption is one of the main design constraints within a sensor node. Ditzel and Elferink [7] have designed a sensor node for RF sensing based applications, which consumes 10mA at 3V and provides a sensing range up to 10m. While working prototypes have already been developed, extensive research is yet to be done in developing reliable and computationally efficient target detectors. Dutta *et al.* [6] have considered Neyman-Pearson based binary hypothesis detector to be a suitable target detector. Meguerdichian *et al.* [11] and Phipatanasuphorn and Ramanathan [12] have proposed a target detector, which uses the average signal strength as measured by the sensor nodes to detect the presence of targets. While such methods are simple to implement and computationally less complex, their target detection reliabilities are poor due to high false alarm rates. In many of the practical surveillance applications, IoT are required to operate in harsh sensing environments and the low complexity target detectors proposed for IoT exhibit increased false detection rates and reduced reliability. Real time experiments on Mica2 motes showed that the false

alarm rates of the decisions taken based on the data from a single sensor can be as high as 60 percent [13]. In [10], authors have proposed an IoT with multiple sensor nodes distributed within the sensing region. Varshney [14] discussed data fusion to improve the target detection reliability. A network of distributed sensor nodes is designed in [15]–[17] where the sensors are grouped together by a control centre which can adopt joint scheduling approach [18]. The distributed network can provide improved sensing coverage and connectivity with efficient energy consumption. A distributed network of sensor nodes can be seen as a multiple-input multiple-output (MIMO) system that transmits a waveform of known shape and detects the reflected echoes from the target. The presence of multiple sensor nodes within the sensing region increases the probability of detecting the presence of targets. However, the signals transmitted from the neighbouring sensor nodes interfere with each other and reduce the target detection reliability. In the existing literature, various target detectors [19]–[24] have been proposed by the authors to provide improved target detection performance. However, the proposed target detectors are computationally intense and incompatible with resource constrained IoT. The presence of objects within the sensing region, which interact with the transmitted signal result in clutter returns. Since, clutter returns appear similar to the target returns, the presence of clutter leads to increased false detection rates and reduced reliability. In this paper, we design a target detector, which operates within the sensing and operational constraints of IoT. The proposed target detector is expected to provide an acceptable trade-of between power consumption, target detection reliability and computational complexity.

III. PROBLEM FORMULATION

We have considered a low power surveillance system, which is supported by IoT. To achieve increased reliability within the low power applications of IoT, we consider RF sensing as the primary means of sensing. The proposed IoT consist of clusters of sensor nodes, which are distributed within the sensing region. Each cluster consists of a control centre and a group of receiving nodes, which are distributed within the sensing region. It is assumed that the control centre is equipped with sufficient resources to transmit the desired RF-signal into the sensing region. The received signal model at the receiving nodes is summarised in Fig. 1. The receiving nodes co-ordinate among themselves to detect the reflected components of the transmitted RF-signal.

Let there be a cluster of N_s sensor nodes. If the signal is transmitted for a time period of T sec $0 \leq t \leq T$, at a sampling rate of f_s, let $\mathbf{s}$ be a $N_t \times 1$ vector representing the time-limited, finite energy transmit signal. Therefore, total energy allocated to each transmission period is

$$E = \int_0^T \mathbf{s}^2(t)dt = \sum_{i=1}^{N_t} \mathbf{s}^2(i) = \mathbf{s}^H\mathbf{s} \tag{1}$$

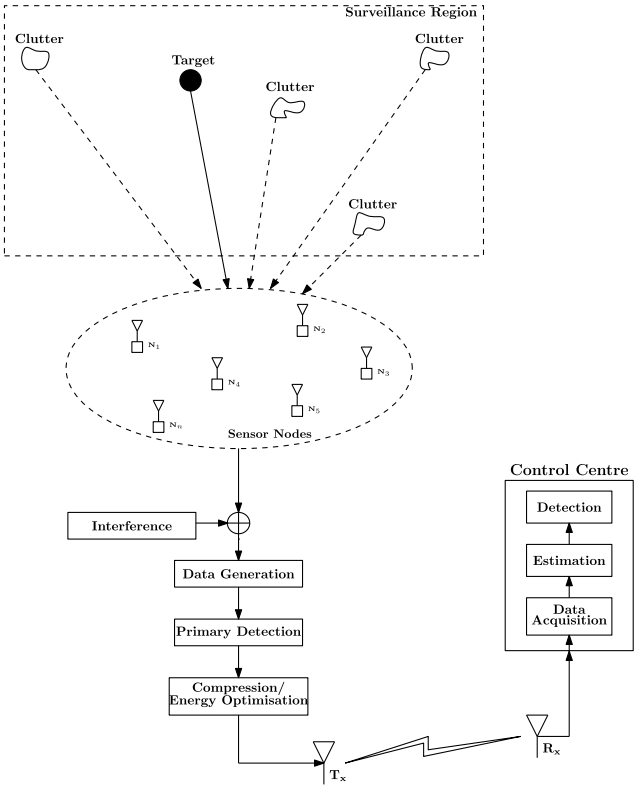

FIGURE 1. Proposed Sensing Scheme for Internet of Things.

When a waveform $\mathbf{s}(t)$ is transmitted, the receiving nodes are expected to receive a direct arrival and reflected components of the transmitted signal where the reflected components are characterised by a time delay. It is assumed that the transmitting and receiving nodes are synchronised so that the reflected signals can be distinguished from the direct arrivals. The sensor nodes also receive interfering signals from the neighbouring clusters. The control centre is assumed to have the knowledge of the transmitting waveforms from the neighbouring clusters. If $\mathbf{y}_i(t)$ is the received signal at the i^{th} sensor node, then we can write,

$$\mathbf{y}_i(t) = \sum_{k=1}^{t_n} \mathbf{s}(t) * \mathbf{a}_{ik}(t) + \sum_{k=1}^{b_n} \mathbf{h}_k(t) * \mathbf{b}_{ik}(t) + \sum_{k=1}^{c_n} \mathbf{c}_{ik}(t) + \mathbf{w}_i(t), \quad 0 \leq t \leq T_y \tag{2}$$

Where $*$ denotes convolution operator. T_y is the total time period over which the received signal samples are collected, $\mathbf{s}(t)$ is the reference transmit waveform, $\mathbf{a}_k(t)$ is the impulse response corresponding to the k^{th} target return and t_n is the number of targets within the range bin. $\mathbf{h}_k(t)$ is the is the k^{th} interfering signal, $\mathbf{b}_k(t)$ is the impulse response corresponding to the k^{th} interfering signal and b_n is the number of interfering nodes. $\mathbf{w}(t)$ is the thermal noise.

Let the impulse response of the target return be negligible for a time duration of T_a. Hence the received signals have to

be observed for an extended duration of time which is given by $T_y = T + T_a$. The discrete $N_y \times 1$ received signal data at the i^{th} sensor node is represented as,

$$\begin{aligned}\mathbf{y}_i[n] &= \sum_{k=1}^{t_n} \mathbf{S}\mathbf{a}_{ik}[n] + \sum_{k=1}^{b_n} \mathbf{H}_k \mathbf{b}_{ik}[n] + \sum_{k=1}^{c_n} \mathbf{c}_{ik}[n] + \mathbf{w}_i[n] \\ \mathbf{a}_i &= [a_1, a_2, \ldots, a_{N_a}]^T, \quad i = 1,2 \ldots N_s \\ \mathbf{b}_i &= [b_1, b_2, \ldots, b_{N_a}]^T, \quad i = 1,2 \ldots N_s \end{aligned} \tag{3}$$

Where $\mathbf{y}_i$ is the $N_y \times 1$ received signal data at the i^{th} receiving node, $N_y = N_t + N_a$ - 1. $\mathbf{a}_i$ is the $N_a \times 1$ unknown impulse response associated with the target return at the i^{th} receiving node; $\mathbf{b}_i$ is the $N_a \times 1$ unknown impulse response of the interfering signal at the i^{th} receiving node; $\mathbf{c}_i$ is the clutter return at the i^{th} receiving node. Noise is assumed to be AWGN with unknown variance. $\mathbf{S}$ is the $N_y \times N_a$ convolution matrix of $\mathbf{s}(t)$, $\mathbf{H}$ is the $N_y \times N_a$ convolution matrix of $\mathbf{h}(t)$ and can be written as in [25], [26],

$$\mathbf{S} = \begin{bmatrix} s(1) & 0 & \ldots & \ldots & 0 \\ s(2) & s(1) & \ddots & \ldots & 0 \\ \vdots & \vdots & \ddots & \ddots & 0 \\ s(N_t) & s(N_t-1) & \ldots & s(1) & 0 \\ 0 & s(N_t) & s(N_t-1) & \ldots & s(1) \\ \vdots & 0 & s(N_t) & \ldots & s(2) \\ \vdots & \vdots & 0 & \ddots & \vdots \\ 0 & 0 & \ldots & 0 & s(N_t) \end{bmatrix} \tag{4}$$

$$\mathbf{H} = \begin{bmatrix} h(1) & h(0) & h(-1) & \ldots & h(2-N_a) \\ h(2) & h(1) & \ddots & \ldots & \vdots \\ \vdots & \vdots & \ddots & \ddots & \vdots \\ h(N_t) & h(N_t-1) & \ldots & h(1) & \vdots \\ \vdots & h(N_t) & h(N_t-1) & \ldots & h(1) \\ \vdots & h(0) & h(N_t) & \ldots & h(2) \\ \vdots & \vdots & h(0) & \ddots & \vdots \\ h(N_y) & h(N_y-1) & h(N_y-2) & h(0) & h(N_t) \end{bmatrix} \tag{5}$$

The convolution matrices $\mathbf{S}$ and $\mathbf{H}$ allow us to denote the continuous time convolution operator $(*)$ in (2) into discrete form. In (3) while the impulse responses $\mathbf{a}$, $\mathbf{b}$ and noise variance are unknown but deterministic however, clutter is unknown. Before proceeding to the target detector design, the problem of unknown clutter has to be addressed.

IV. CLUTTER ESTIMATION

We consider clutter to be comprised of all the fixed scatterers within the sensing region. Due to the nature of sensor nodes with short range sensing capabilities, the dominant scatterers that contribute to clutter are assumed to be non-varying over extended periods of time. The cluttered nature of the sensing environment produces additional transmit signal echoes, which arrive at the sensor nodes along with the target returns. The vector $\mathbf{c}_i$ in (3) is a $N_y \times 1$ vector containing the clutter returns. In the existing literature, authors have proposed modelling clutter as a Compound-Gaussian process [27]–[29] i.e., as a product of two independent random variables.

$$\mathbf{c} = \sqrt{\varsigma}\mathbf{g} \tag{6}$$

Here the speckle, $\mathbf{g}$ is a complex Gaussian with covariance matrix $\mathbf{\Sigma}$ and ς is the clutter texture component and is usually a real nonnegative scalar. Kraut *et al.* [30]–[32] and Scharf and McWhorter [33] have addressed the problem of target detection in the presence of clutter with known covariance structure but unknown level. However, the presence of a noise component whose power is independent of clutter is largely ignored. We consider a disturbance vector consisting of noise and clutter signals, which can be estimated from secondary data,

$$\mathbf{n} = \sqrt{\varsigma}\mathbf{g} + \mathbf{w} \tag{7}$$

$$\mathbf{R}_d = \varsigma\mathbf{\Sigma} + \sigma^2\mathbf{I} \tag{8}$$

Where $\mathbf{n}$ is the disturbance vector and $\mathbf{R}_d$ is the disturbance covariance matrix. $\mathbf{I}$ is a $M \times M$ identity matrix where M is the length of the received signal vector. $\mathbf{\Sigma}$ is the clutter covariance matrix which is unknown to the target detector. Noise variance σ^2 is deterministic and unknown. Estimation of these unknown parameters is addressed in the later sections. Clutter covariance estimation has been addressed by the authors in the existing literature [34]–[36]. If clutter texture is gamma-distributed with mean μ and order ν, texture distribution function can be written as,

$$f(\varsigma) = \frac{1}{\Gamma(\nu)}\left(\frac{\nu}{\mu}\right)^{\nu} \varsigma^{\nu-1} e^{-\frac{\nu}{\mu}\varsigma} \quad \varsigma \geq 0 \tag{9}$$

Where $\Gamma(\nu)$ is the gamma function of order ν. The unconditional probability density function (pdf) of the disturbance vector $\mathbf{n}$ can be obtained by averaging $f(\mathbf{n}|\varsigma)$ with respect to its texture distribution $f(\varsigma)$ [37].

$$f(\mathbf{n}) = \int_0^{\infty} \frac{1}{\pi^{N_y N_s} |\varsigma\mathbf{\Sigma} + \sigma^2\mathbf{I}|} \times exp\left[-\mathbf{n}^H (\varsigma\mathbf{\Sigma} + \sigma^2\mathbf{I})^{-1}\mathbf{n}^H \right] f(\varsigma) d\varsigma \tag{10}$$

However, the detection strategy based on this clutter model is difficult to implement within resource constrained IoT as it involves unknown parameters and computationally intense numerical integrations with respect to clutter texture distribution. It can be recalled that the disturbance covariance matrix $\mathbf{R}_d$ is the sum of unknown stationary clutter and random deterministic noise. We now derive a simple strategy to estimate clutter from the disturbance covariance matrix. The clutter covariance matrix, $\varsigma\mathbf{\Sigma}$ is assumed to have a known structure whose rank r is significantly less than M which is usually true in many practical applications.

Let λ_{di} and $\mathbf{\Phi}_{di}$ $(i = 1, 2 \ldots M)$ be the i^{th} eigenvalue and the corresponding i^{th} normalised eigenvector respectively

of the disturbance covariance matrix $\mathbf{R}_d$. Since $\mathbf{R}_d$ is symmetric, the disturbance covariance matrix can be expressed as $\mathbf{\Phi}_d\boldsymbol{\lambda}_d\mathbf{\Phi}_d^H$. Similarly let λ_{ci} and $\mathbf{\Phi}_{ci}$ be the i^{th} eigenvalue and the corresponding i^{th} normalised eigenvector respectively of the clutter covariance matrix $\mathbf{\Sigma}$. It must be noted that $\boldsymbol{\lambda}_c$ and $\mathbf{\Phi}_c$ here are unknown. From (8) $\boldsymbol{\lambda}_d$ can be written as, $\boldsymbol{\lambda}_d = \varsigma\boldsymbol{\lambda}_c + \sigma^2\mathbf{I}$. Therefore, $\mathbf{R}_d$ can be expressed as,

$$\mathbf{R}_d = \mathbf{\Phi}_d(\varsigma\boldsymbol{\lambda}_c + \sigma^2\mathbf{I})\mathbf{\Phi}_d^H \tag{11}$$

Finally, inverse covariance matrix is given by,

$$\begin{aligned}\mathbf{R}_d^{-1} &= (\mathbf{\Phi}_d^H)^{-1}(\varsigma\boldsymbol{\lambda}_c + \sigma^2\mathbf{I})^{-1}(\mathbf{\Phi}_d)^{-1}\\ &= \mathbf{\Phi}_d(\varsigma\boldsymbol{\lambda}_c + \sigma^2\mathbf{I})^{-1}\mathbf{\Phi}_d^H\end{aligned} \tag{12}$$

To solve (12), we need to obtain the inverse of $(\varsigma\boldsymbol{\lambda}_c + \sigma^2\mathbf{I})$. Clearly $(\sigma^2\mathbf{I})^{-1}$ and $(\varsigma\boldsymbol{\lambda}_c+\sigma^2\mathbf{I})^{-1}$ always exist. Fundamental matrix inversion lemma may be used to solve this problem if the rank of $\boldsymbol{\lambda}_c$ is 1. However, based on our previous assumption, when the rank of $\boldsymbol{\lambda}_c$ is r such that $1 \leq r \ll \mathrm{M}$. Therefore, matrix inversion lemma may not always be applicable. When $\sigma^2\mathbf{I}$ and $(\sigma^2\mathbf{I} + \varsigma\boldsymbol{\lambda}_c)$ are non-singular, from [38] inverse of $(\sigma^2\mathbf{I} + \varsigma\boldsymbol{\lambda}_c)$ is given by,

$$\begin{aligned}(\sigma^2\mathbf{I} + \varsigma\boldsymbol{\lambda}_c)^{-1} &= \boldsymbol{\kappa}_r^{-1} - v_r\boldsymbol{\kappa}_r^{-1}\boldsymbol{\delta}_r\boldsymbol{\kappa}_r^{-1}\\ v_k &= \frac{1}{1 + tr(\boldsymbol{\kappa}_k^{-1}\boldsymbol{\delta}_k)}\\ \boldsymbol{\kappa}_{k+1}^{-1} &= \boldsymbol{\kappa}_k^{-1} - v_k\boldsymbol{\kappa}_k^{-1}\boldsymbol{\delta}_k\boldsymbol{\kappa}_k^{-1}\end{aligned} \tag{13}$$

Where $\boldsymbol{\kappa}_1 = \sigma^2\mathbf{I}$; Following the results from [38], the matrix $\varsigma\boldsymbol{\lambda}_c$ can be decomposed into a sum of matrices of rank one i.e., $\varsigma\boldsymbol{\lambda}_c = \sum_{i=1}^{r}\boldsymbol{\delta}_i$ and rank of $\boldsymbol{\delta}_i$ is one. Solving (12) and (13) recursively gives us the inverse of the disturbance covariance matrix as,

$$\mathbf{R}_d^{-1} = \sigma^{-2}\mathbf{C} \tag{14}$$

Detailed explanation is given in Appendix. Here $\mathbf{C}$ is the clutter projection matrix given by,

$$\mathbf{C} \approx \mathbf{I} - \sum_{i=1}^{r}\mathbf{\Phi}_{di}\mathbf{\Phi}_{di}^H \tag{15}$$

When clutter returns are significantly stronger than the noise power, the dominant eigenvalues in $\boldsymbol{\lambda}_d$ which correspond to the clutter returns can be easily distinguished from the remaining eigenvalues of $\boldsymbol{\lambda}_d$. The clutter projection matrix $\mathbf{C}$ can be easily obtained from the eigenvectors corresponding to the dominant eigen values of $\mathbf{R}_d$.

V. TARGET DETECTOR DESIGN

The performance measure of IoT as a surveillance system; while dedicated to detecting the existence or non-existence of targets, is the degree of reliability on such decision-making process. The two possible outcomes of this decision making process are occurrence and non-occurrence of the target which is modelled as a binary hypothesis testing problem. The two possible hypotheses are H_0 and H_1; where H_0 represents the absence of a target and H_1 represents the presence of a target. The received signal models corresponding to these hypothesis H_0 and H_1 at the control centre are,

$$\begin{aligned}H_0 &: \mathbf{y}[n] = \sum_{k=1}^{b_n}\mathbf{H}_k\mathbf{b}_k[n] + \mathbf{n}[n]\\ H_1 &: \mathbf{y}[n] = \sum_{k=1}^{t_n}\mathbf{S}\mathbf{a}_k[n] + \sum_{k=1}^{b_n}\mathbf{H}_k b_k[n] + \mathbf{n}[n]\end{aligned} \tag{16}$$

Here, $\mathbf{a} = [a_1, a_2, \ldots, a_{N_s}]^T$ and $\mathbf{b} = [b_1, b_2, \ldots, b_{N_s}]^T$. Our objective is to develop a target detector which has the ability to make a distinction between hypothesis H_0 and H_1 based on the received signal samples which are corrupted by noise, clutter and interfering signals. A test statistic is generated which is measured against a predefined threshold based on which a decision is made regarding the existence or absence of a target. The test statistic for the proposed target detector is generated from the likelihood ratio function within which the unknown parameters are estimated using Maximum Likelihood Estimator (MLE). The threshold γ is generated such that the maximum false alarm rate is restricted to a permissible limit. To design a target detector, the pdfs of the received signal samples $\mathbf{y}[n]$ under hypothesis H_0 and H_1 is required to be defined. Using the inverse covariance estimate from (14), the pdfs under hypothesis H_0 (17) and H_1 (17) are written as,

$$\begin{aligned}&f(\mathbf{y}|\mathbf{b}, \sigma^2, H_0)\\ &= \frac{1}{(\pi\sigma^2)^{N_yN_s}|\mathbf{C}^{-1}|}\\ &\quad\times exp\left[\frac{-1}{\sigma^2}\left((\mathbf{y} - \sum_{k=1}^{b_n}\mathbf{H}_k\mathbf{b}_k)^H\mathbf{C}(\mathbf{y} - \sum_{k=1}^{b_n}\mathbf{H}_k\mathbf{b}_k)\right)\right]\end{aligned} \tag{17}$$

$$\begin{aligned}&f(\mathbf{y}|\mathbf{a}, \mathbf{b}, \sigma^2, H_1)\\ &= \frac{1}{(\pi\sigma^2)^{N_yN_s}|\mathbf{C}^{-1}|}exp\left[\frac{-1}{\sigma^2}\left((\mathbf{y} - \sum_{k=1}^{t_n}\mathbf{S}\mathbf{a}_k\right.\right.\\ &\quad\left.\left. - \sum_{k=1}^{b_n}\mathbf{H}_k\mathbf{b}_k)^H\mathbf{C}(\mathbf{y} - \sum_{k=1}^{t_n}\mathbf{S}\mathbf{a}_k - \sum_{k=1}^{b_n}\mathbf{H}_k\mathbf{b}_k)\right)\right]\end{aligned} \tag{18}$$

Case 1 (Detector Design With Known σ^2 and 1 Interfering Node): In this case we assume that the noise variance is known to that target detector and only one neighbouring sensor node is contributing to interference i.e., $b_n = 1$. This is applicable to the scenario where sensor nodes are widely scattered and the interference from the other sensor nodes is negligibly weak. The test statistic, $\mathbb{T}$ for the proposed target detector is obtained from the pdfs defined in (17) and (18) where the unknown parameters are replaced by their MLEs as,

$$\mathbb{T} = \frac{\max\limits_{\mathbf{a},\mathbf{b}} f(\mathbf{y}|\mathbf{a}, \mathbf{b}, H_1)}{\max\limits_{\mathbf{b}} f(\mathbf{y}|\mathbf{b}, H_0)} \underset{H_0}{\overset{H_1}{\gtrless}} \gamma \tag{19}$$

The MLEs of the unknown parameters are obtained by differentiating the exponential arguments of the pdfs

in (17) and (18) with respect to the corresponding unknown parameter. The corresponding derivatives under hypothesis H_0 and H_1 are equated to zero to obtain the ML estimate. Since $\mathbf{C}$ is Hermitian, differentiating the exponential term in the (18) with respect to $\mathbf{b}$ gives us,

$$\mathbf{H}^H\mathbf{C}\mathbf{H}\hat{\mathbf{b}}_1 = \mathbf{H}^H\mathbf{C}\mathbf{y} - \mathbf{H}^H\mathbf{C}\mathbf{S}\sum_{k=1}^{t_n}\hat{\mathbf{a}}_k \tag{20}$$

Here, $\hat{\mathbf{b}}_1$ denotes the ML estimate of interference impulse response under hypothesis H_1 and $\hat{\mathbf{a}}$ represents the ML estimate of the target impulse response, which is unknown at this stage. Similarly, from (17) the ML estimate of $\mathbf{b}$ under hypothesis H_0 can be obtained as,

$$\mathbf{H}^H\mathbf{C}\mathbf{H}\hat{\mathbf{b}}_0 = \mathbf{H}^H\mathbf{C}\mathbf{y} \tag{21}$$

Here, $\hat{\mathbf{b}}_0$ denotes the ML estimate of $\mathbf{b}$ under hypothesis H_0. With the knowledge of the transmit and the interfering waveforms available to the control centre, the reference correlation matrices are written as,

$$\mathbf{R_s} = \mathbf{S}^H\mathbf{C}\mathbf{S} \tag{22}$$
$$\mathbf{R_h} = \mathbf{H}^H\mathbf{C}\mathbf{H} \tag{23}$$

$\mathbf{R_s}$ and $\mathbf{R_h}$ can be interpreted as the transmit and interfering signal correlation matrices respectively. Similarly we define $\mathbf{R_{hs}}$ which is the reference cross-correlation matrix between the transmit and the interfering signals as,

$$\mathbf{R_{hs}} = \mathbf{H}^H\mathbf{C}\mathbf{S} \tag{24}$$

Finally, we define the cross-correlation matrices for received signal with respect to the transmit and the interfering signals as $\mathbf{R_{sy}}$ and $\mathbf{R_{hy}}$ which are given by,

$$\mathbf{R_{hy}} = \mathbf{H}^H\mathbf{C}\mathbf{y} \tag{25}$$
$$\mathbf{R_{sy}} = \mathbf{S}^H\mathbf{C}\mathbf{y} \tag{26}$$

Using the correlation matrices, (20) and (21) can be rewritten as,

$$\mathbf{R_h}\hat{\mathbf{b}}_1 = \mathbf{R_{hy}} - \mathbf{R_{hs}}\hat{\mathbf{a}} \tag{27}$$
$$\mathbf{R_h}\hat{\mathbf{b}}_0 = \mathbf{R_{hy}} \tag{28}$$

Using (27), the ML estimate of the unknown target impulse response is obtained by differentiating the exponential argument in (18) with respect to $\mathbf{a}$ and equating it to zero. Solving this differential equation gives us,

$$\mathbf{S}^H\mathbf{Q}\mathbf{S}\sum_{k=1}^{t_n}\hat{\mathbf{a}}_k = \mathbf{S}^H\mathbf{Q}\mathbf{y} \tag{29}$$

$$\mathbf{Q} = \left(\mathbf{I} - \mathbf{H}\mathbf{R_h}^{-1}\mathbf{H}^H\mathbf{C}\right)^H\mathbf{C}\left(\mathbf{I} - \mathbf{H}\mathbf{R_h}^{-1}\mathbf{H}^H\mathbf{C}\right) \tag{30}$$

Here, $\hat{\mathbf{a}}$ represents the ML estimate of the target impulse response under hypothesis H_1. The test statistic for the proposed target detector in this case is obtained from (19) as,

$$\mathbb{T} = exp\Bigg[\frac{-1}{\sigma^2}\Bigg(\Big(\mathbf{y} - \sum_{k=1}^{t_n}\mathbf{S}\hat{\mathbf{a}}_k - \mathbf{H}\hat{\mathbf{b}}_1\Big)^H\mathbf{C}\Big(\mathbf{y} - \sum_{k=1}^{t_n}\mathbf{S}\hat{\mathbf{a}}_k - \mathbf{H}\hat{\mathbf{b}}_1\Big) - \big(\mathbf{y} - \mathbf{H}\hat{\mathbf{b}}_0\big)^H\mathbf{C}\big(\mathbf{y} - \mathbf{H}\hat{\mathbf{b}}_0\big)\Bigg)\Bigg]_{H_0}^{\overset{H_1}{\geq}\gamma} \tag{31}$$

To solve (31) we apply logarithm on both sides, and use the correlation matrices defined in equations (23) to (26) which gives us the desired test statistic,

$$ln\ \mathbb{T} = \frac{-1}{\sigma^2}\Bigg(\hat{\mathbf{a}}^H{\mathbf{R_{hs}}}^H{\mathbf{R_h}}^{-1}\mathbf{R_{hs}}\hat{\mathbf{a}} - {\mathbf{R_{sy}}}^H\hat{\mathbf{a}} - \hat{\mathbf{a}}^H\mathbf{R_{sy}} + \times\hat{\mathbf{a}}^H\mathbf{R_s}\hat{\mathbf{a}} + {\mathbf{R_{hy}}}^H\hat{\mathbf{b}}_1 + \hat{\mathbf{b}}_1^H\mathbf{R_{hy}} - 2\hat{\mathbf{b}}_1^H\mathbf{R_h}\hat{\mathbf{b}}_1\Bigg)_{H_0}^{\overset{H_1}{\geq}} ln\ \gamma \tag{32}$$

To optimise the test statistic derived in (32), we adopt a two-stage target detection model. The proposed two-stage design model for IoT is summarised in Fig. 2. Considering the operational nature of IoT with static clutter and known interfering waveforms, we perform target detection in two stages which are, 1) Initialisation stage and 2) Operational stage as shown in Fig. 3. In the initialisation stage, the known knowledge of clutter and interference statistics are exploited to generate the measurement and test statistic coefficients. Since the sensing conditions are expected to be static over a significant period of time, the initialisation stage is only required to be performed periodically. In the operational stage, the received signal data is used along with the test statistic coefficients to generate the actual measurable test statistic based on which a final decision is made regarding the existence or absence of the target. The measurement coefficients which are be estimated during the initialisation stage can be expressed as,

$$\begin{bmatrix} \boldsymbol{\nabla}_1 & \boldsymbol{\nabla}_2 \\ \boldsymbol{\nabla}_3 & \boldsymbol{\nabla}_4 \end{bmatrix} = \begin{bmatrix} (\mathbf{Q}\mathbf{S})(\mathbf{S}^H\mathbf{Q}\mathbf{S})^{-1} & \mathbf{R_h}^{-1}\mathbf{H}^H\mathbf{C} \\ \boldsymbol{\nabla}_1{\mathbf{R_{hs}}}^H\boldsymbol{\nabla}_2 & \boldsymbol{\nabla}_1\mathbf{S}^H\mathbf{C} \end{bmatrix} \tag{33}$$

Using the ML estimates of $\hat{\mathbf{a}}$ and $\hat{\mathbf{b}}$ and the measurement coefficients in (33), the optimised test statistic for the proposed target detector can be obtained as,

$$ln\ \mathbb{T} = \mathbf{y}^H\boldsymbol{\chi}\mathbf{y}\underset{H_1}{\overset{H_0}{\gtrless}} - \sigma^2 ln\ \gamma \tag{34}$$

$$\boldsymbol{\chi} = (\boldsymbol{\nabla}_3^H + \boldsymbol{\nabla}_3) - (\boldsymbol{\nabla}_4^H + \boldsymbol{\nabla}_4) - (\boldsymbol{\nabla}_3 - \boldsymbol{\nabla}_4)\mathbf{C}^{-1}\boldsymbol{\nabla}_4^H \tag{35}$$

Where $\boldsymbol{\chi}$ is the test statistic coefficient. Since $\boldsymbol{\chi}$ and the measurement coefficients are independent of the received signal data, they can be generated during the initialisation stage which reduces the computational complexity during the operational stage.

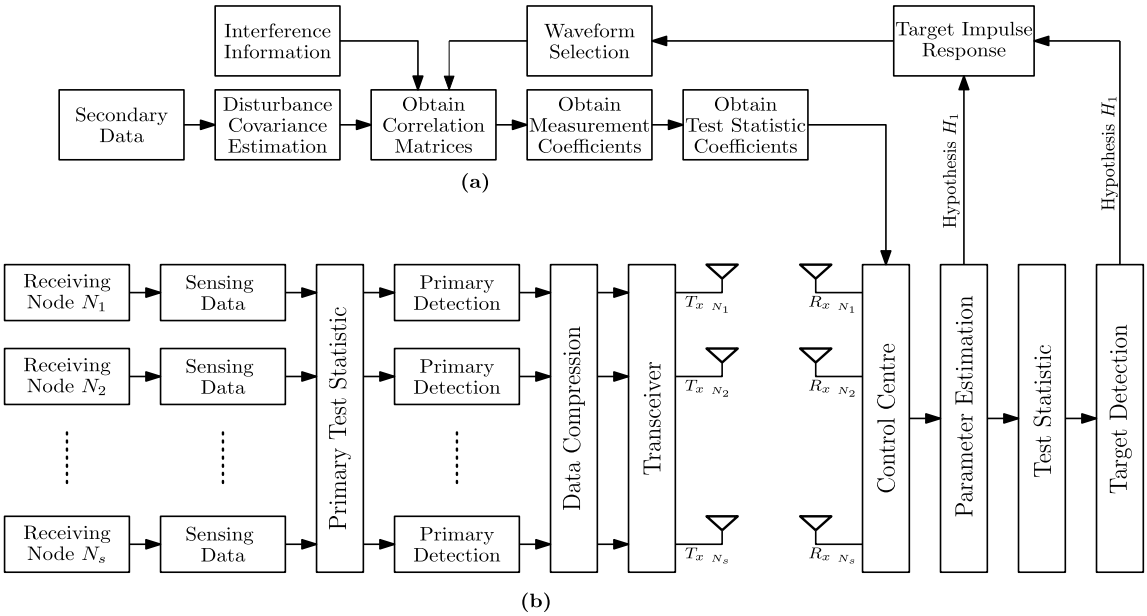

FIGURE 2. Proposed RF sensing Based IoT for Surveillance Applications. (a) Measurement of Estimation Coefficients in Initialisation stage. (b) Proposed Target detection Architecture in Operational Stage.

Case 2 (Detector Design With Unknown σ^2 and 1 Interfering Node): In this case, we assume that the noise variance is unknown to the target detector. We consider the presence of only one interfering node. The estimates of the unknown parameters $\mathbf{a}$ and $\mathbf{b}$ are obtained as explained in (27) to (29). The ML estimates of σ^2 under hypothesis H_0 and H_1 are obtained by differentiating (17) and (18) respectively with respect to σ^2 as,

$$\hat{\sigma}_0^2 = \frac{1}{N_y N_s}\left(\mathbf{y}^H\mathbf{C}\mathbf{y} - \mathbf{R_{hy}}^H\hat{\mathbf{b}}_0 - \hat{\mathbf{b}}_0^H\mathbf{R_{hy}} - \hat{\mathbf{b}}_0^H\mathbf{R_h}\hat{\mathbf{b}}_0\right) \quad (36)$$

$$\hat{\sigma}_1^2 = \frac{1}{N_y N_s}\Big(\mathbf{y}^H\mathbf{C}\mathbf{y} - \mathbf{R_{sy}}^H\hat{\mathbf{a}} - \mathbf{R_{hy}}^H\hat{\mathbf{b}}_1 + \hat{\mathbf{a}}^H\big(\mathbf{R_s}\hat{\mathbf{a}} + \mathbf{R_{hs}}^H\hat{\mathbf{b}}_1 - \mathbf{R_{sy}}\big) + \hat{\mathbf{b}}_1^H\big(\mathbf{R_{hs}}\hat{\mathbf{a}} + \mathbf{R_h}\hat{\mathbf{b}}_1 - \mathbf{R_{hy}}\big)\Big) \quad (37)$$

Here, $\hat{\sigma}_0^2$ and $\hat{\sigma}_1^2$ are the MLEs of noise variance under hypothesis H_0 and H_1 respectively. Using $\hat{\sigma}^2$, $\hat{\mathbf{a}}$ and $\hat{\mathbf{b}}$, the test statistic for the proposed target detector is written as,

$$\mathbb{T} = \frac{\max\limits_{\sigma^2,\mathbf{a},\mathbf{b}} f(\mathbf{y}|\mathbf{a},\mathbf{b},\sigma^2,H_1)}{\max\limits_{\sigma^2,\mathbf{b}} f(\mathbf{y}|\mathbf{b},\sigma^2,H_0)} = \left(\frac{\hat{\sigma}_0^2}{\hat{\sigma}_1^2}\right)^{N_y N_s} \underset{H_0}{\overset{H_1}{\gtrless}} \gamma \quad (38)$$

Substituting $\hat{\sigma}_0^2$ and $\hat{\sigma}_1^2$ and correlation matrices defined in equations (23) to (26) gives the desired test statistic as,

$$\mathbb{T} = \frac{q_0}{q_1} \underset{H_0}{\overset{H_1}{\gtrless}} \sqrt[N_y N_s]{\gamma} \quad (39)$$

Where q_0 and q_1 are given by,

$$q_0 = \mathbf{y}^H\mathbf{C}\mathbf{y} - \mathbf{R_{hy}}^H\mathbf{R}_h^{-1}\mathbf{R_{hy}} \quad (40)$$

$$q_1 = \mathbf{y}^H\mathbf{C}\mathbf{y} - \mathbf{R_{hy}}^H\mathbf{R}_h^{-1}\mathbf{R_{hy}} + \hat{\mathbf{a}}^H\mathbf{R_{hs}}^H\mathbf{R}_h^{-1}\mathbf{R_{hs}}\hat{\mathbf{a}} - \mathbf{R_{sy}}^H\hat{\mathbf{a}} - \hat{\mathbf{a}}^H\mathbf{R_{sy}} + \hat{\mathbf{a}}^H\mathbf{R_s}\hat{\mathbf{a}} + \mathbf{R_{hy}}^H\hat{\mathbf{b}}_1 + \hat{\mathbf{b}}_1^H\mathbf{R_{hy}} - 2\hat{\mathbf{b}}_1^H\mathbf{R_h}\hat{\mathbf{b}}_1 \quad (41)$$

To optimise the test statistic in (39), we now solve (40) and (41) by using the measurement coefficients defined in (33). This leads us to generating the test statistic coefficients given by,

$$\boldsymbol{\chi}_0 = \mathbf{C} - \boldsymbol{\nabla}_2^H\mathbf{R_h}\boldsymbol{\nabla}_2 \quad (42)$$

$$\boldsymbol{\chi}_1 = \boldsymbol{\chi}_0 + (\boldsymbol{\nabla}_3^H + \boldsymbol{\nabla}_3) - (\boldsymbol{\nabla}_4^H + \boldsymbol{\nabla}_4) - (\boldsymbol{\nabla}_3 - \boldsymbol{\nabla}_4)\mathbf{C}^{-1}\boldsymbol{\nabla}_4^H \quad (43)$$

Here, $q_0 = \mathbf{y}^H\boldsymbol{\chi}_0\mathbf{y}$ and $q_1 = \mathbf{y}^H\boldsymbol{\chi}_1\mathbf{y}$. Therefore, the optimised test statistic for the proposed target detector is,

$$\mathbb{T} = \left(\frac{\mathbf{y}^H\boldsymbol{\chi}_0\mathbf{y}}{\mathbf{y}^H\boldsymbol{\chi}_1\mathbf{y}}\right) \underset{H_0}{\overset{H_1}{\gtrless}} \sqrt[N_y N_s]{\gamma} \quad (44)$$

Case 3 (Detector Design With Unknown σ^2 and n Interfering Nodes): Here we design a target detector for a generalised scenario with unknown noise variance and multiple interfering nodes i.e., $b_n = n$. Since the interfering waveforms are mutually independent, estimating the unknown impulse responses from each interfering waveform allows us to dynamically adopt to any changes in the choice of transmit waveforms within the neighbourhood of the sensor node. The pdfs of the received signal under hypothesis H_0 (45) and

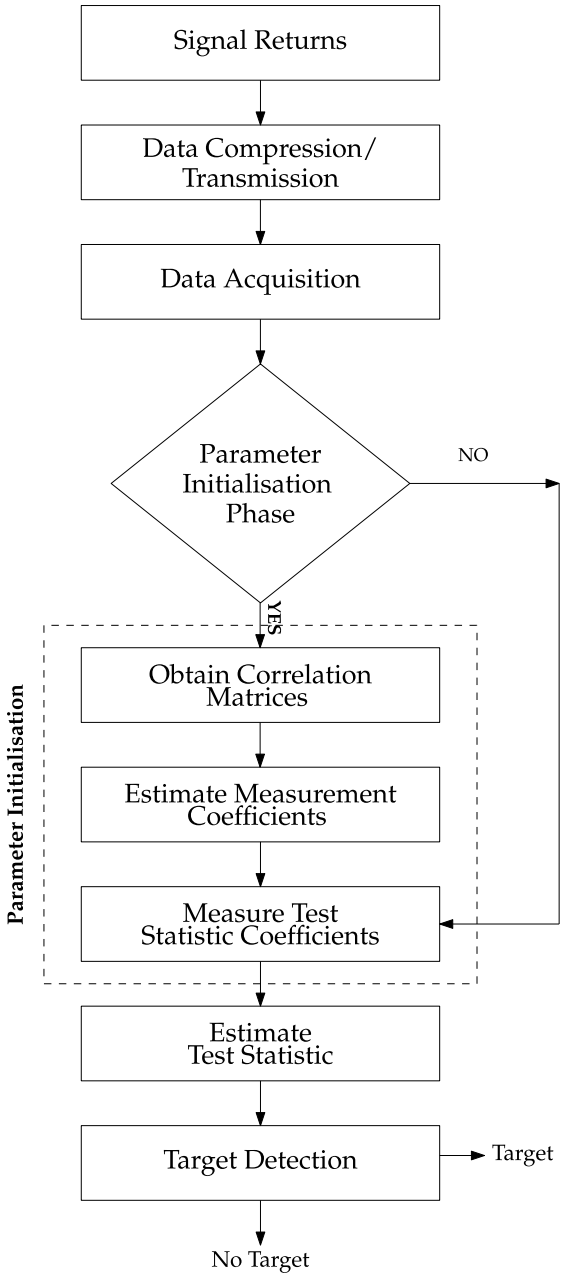

FIGURE 3. Operational Principle of the Proposed 2-Stage Target Detection Model.

H_1 (46) are given by,

$$f(\bar{\mathbf{y}}|\mathbf{b}_1, \mathbf{b}_2 \dots \mathbf{b}_n, \sigma^2, H_0) = \frac{1}{(\pi\sigma^2)^{N_y N_s}|\mathbf{C}^{-1}|} \times exp\left[\frac{-1}{\sigma^2}\left((\mathbf{y} - \sum_{k=1}^{b_n}\mathbf{H}_k\mathbf{b}_k)^H\mathbf{C}(\mathbf{y} - \sum_{k=1}^{b_n}\mathbf{H}_k\mathbf{b}_k)\right)\right] \quad (45)$$

$$f(\bar{\mathbf{y}}|\mathbf{b}_1, \mathbf{b}_2 \dots \mathbf{b}_n, \mathbf{a}, \sigma^2, H_1) = \frac{1}{(\pi\sigma^2)^{N_y N_s}|\mathbf{C}^{-1}|} exp\left[\frac{-1}{\sigma^2}\left((\mathbf{y} - \sum_{k=1}^{t_n}\mathbf{S}\mathbf{a}_k - \sum_{k=1}^{b_n}\mathbf{H}_k\mathbf{b}_k)^H\mathbf{C} \times (\mathbf{y} - \sum_{k=1}^{t_n}\mathbf{S}\mathbf{a}_k - \sum_{k=1}^{b_n}\mathbf{H}_k\mathbf{b}_k)\right)\right] \quad (46)$$

The test statistic for the proposed detector in this scenario can be written as,

$$\mathbb{T} = \frac{\max\limits_{\sigma^2, \mathbf{a}, \mathbf{b_1}, \mathbf{b_2} \dots \mathbf{b_n}} f(\mathbf{y}|\sigma^2, \mathbf{a}, \mathbf{b}_1, \mathbf{b}_2 \dots \mathbf{b}_n, H_1)}{\max\limits_{\sigma^2, \mathbf{b_1}, \mathbf{b_2} \dots \mathbf{b_n}} f(\mathbf{y}|\sigma^2, \mathbf{b}_1, \mathbf{b}_2 \dots \mathbf{b}_n, H_0)} \quad (47)$$

The unknown estimates of $\mathbf{b}_1, \mathbf{b}_2 \dots \mathbf{b}_n$ under hypothesis H_0 and H_1 are obtained by performing the procedure described in (20) and (21) recursively for each interfering waveform. However, this requires us to solve a complex n^{th} order differential equation which is computationally intense. Since it is necessary to estimate each interfering signal independently, to obtain a generalised solution we define recursive correlation matrices for the j^{th} interfering signal as,

$$\begin{bmatrix}\mathbf{R}_{\mathbf{h}jk}\\ \mathbf{R}_{\mathbf{h}js}\\ \mathbf{R}_{\mathbf{h}jy}\end{bmatrix} = \mathbf{H}_j^H\mathbf{K}_j\begin{bmatrix}\mathbf{H}_k\\ \mathbf{S}\\ \mathbf{y}\end{bmatrix} \quad (48)$$

Here, $\mathbf{K}_j$ is the projection matrix for j^{th} interfering signal which is measured as,

$$\mathbf{K}_j = (\prod_{l=1}^{j}\mathbf{M}_{l-1})^H\mathbf{C}(\prod_{l=1}^{j}\mathbf{M}_{l-1}) \quad (49)$$

$$\mathbf{M}_n = \mathbf{I} - \mathbf{H}_n\mathbf{R}_{\mathbf{h}nn}^{-1}\mathbf{H}_n^H\mathbf{K}_n \quad \text{n}\neq 0 \quad (50)$$

$$\mathbf{M}_0 = \mathbf{I} \quad (51)$$

Generalised solutions for the recursive impulse response estimates of the j^{th} interfering signal under hypothesis H_0 and H_1 are written as,

$$\begin{aligned}\hat{\mathbf{b}}_{j0} &= (\mathbf{H}_j^H\mathbf{K}_j\mathbf{H}_j)^{-1}\mathbf{H}_j^H\mathbf{K}_j(\mathbf{y} - \sum_{k=j+1}^{n}\mathbf{H}_k\hat{\mathbf{b}}_k)\\ &= \mathbf{R}_{\mathbf{h}jj}^{-1}(\mathbf{R}_{\mathbf{h}jy} - \sum_{k=j+1}^{n}\mathbf{R}_{\mathbf{h}jk}\hat{\mathbf{b}}_k) \quad (52)\\ \hat{\mathbf{b}}_{j1} &= (\mathbf{H}_j^H\mathbf{K}_j\mathbf{H}_j)^{-1}\mathbf{H}_j^H\mathbf{K}_j(\mathbf{y} - \mathbf{S}\hat{\mathbf{a}} - \sum_{k=j+1}^{n}\mathbf{H}_k\hat{\mathbf{b}}_k)\\ &= \mathbf{R}_{\mathbf{h}jj}^{-1}(\mathbf{R}_{\mathbf{h}jy} - \mathbf{R}_{\mathbf{h}sj}\hat{\mathbf{a}} - \sum_{k=j+1}^{n}\mathbf{R}_{\mathbf{h}jk}\hat{\mathbf{b}}_k) \quad (53)\end{aligned}$$

Substituting the results in (45) and (46) respectively and subsequent mathematical analysis reveals that a simple generalised solution for the respective pdfs can be obtained which are rewritten as,

$$f(\mathbf{y}|\sigma^2, H_0) = \frac{1}{(\pi\sigma^2)^{N_y N_s}|\mathbf{C}^{-1}|} exp\left[\frac{-1}{\sigma^2}\left(\mathbf{y}^H\mathbf{K}_{n+1}\mathbf{y}\right)\right] \quad (54)$$

$$f(\mathbf{y}|\mathbf{a}, \sigma^2, H_1) = \frac{1}{(\pi\sigma^2)^{N_y N_s}|\mathbf{C}^{-1}|} \times exp\left[\frac{-1}{\sigma^2}\left((\mathbf{y} - \sum_{k=1}^{t_n}\mathbf{S}\mathbf{a}_k)^H\mathbf{K}_{n+1}(\mathbf{y} - \sum_{k=1}^{t_n}\mathbf{S}\mathbf{a}_k)\right)\right] \quad (55)$$

From (49), the subscript $n+1$ for the interference projection matrix $\mathbf{K}$ is chosen to accommodate all n interfering waveforms. The interference projection matrix can be obtained during the initialisation stage using the known information regarding clutter and interfering waveforms. Hence, the number of interfering nodes has no impact on the computational complexity of the target detection procedure during the operational stage. The control centre gathers the received signal data from all the sensor nodes within its cluster to detect the existence of targets. The amount of power consumed during the data transmission procedure between the sensor nodes and the control centre has a significant impact on the lifetime of the sensor nodes. To reduce the transmission costs, we consider compressive sensing where the sensor nodes are only required to transmit compressed received signal samples to the control centre. The received signal data at the i^{th} sensor node is compressed by projecting it onto a measurement matrix $\boldsymbol{\phi}_i$ such that $\bar{\mathbf{y}}_i = \boldsymbol{\phi}_i \mathbf{y}_i$, where $\bar{\mathbf{y}}_i$ represents the compressed data. The dimensions $M \times N_y$ of $\boldsymbol{\phi}_i$ are chosen such that $M \ll N_y$. $\boldsymbol{\phi}_i$ is usually orthogonal i.e., $\boldsymbol{\phi}_i \boldsymbol{\phi}_i^H = \mathbf{I}$. We define compression ratio $\mu = \frac{M}{N_y}$ which is a measure of compressibility. The choice of compression ratio μ is chosen as a trade-off between the transmission costs and target detection reliability. The compressed received signal data at the control centre can be written as,

$$\begin{aligned}\bar{\mathbf{y}} &= [\bar{\mathbf{y}}_1, \bar{\mathbf{y}}_2, \ldots, \bar{\mathbf{y}}_{Ns}]^T \\ &= \boldsymbol{\phi}[\mathbf{y}_1, \mathbf{y}_2, \ldots, \mathbf{y}_{Ns}]^T \\ \boldsymbol{\phi} &= \begin{bmatrix} \boldsymbol{\phi}_1 & 0 & \ldots & 0 \\ 0 & \boldsymbol{\phi}_2 & \ddots & 0 \\ \vdots & 0 & \ddots & \vdots \\ 0 & \ldots & 0 & \boldsymbol{\phi}_{Ns} \end{bmatrix}\end{aligned} \tag{56}$$

Therefore, the pdfs under hypothesis H_0 and H_1 with the compressed received signal samples are,

$$f(\bar{\mathbf{y}}|\sigma^2, H_0) = \frac{1}{(\pi\sigma^2)^{MN_s}|\mathbf{C}^{-1}|} exp\left[\frac{-1}{\sigma^2}\left(\bar{\mathbf{y}}^H \boldsymbol{\phi}\mathbf{K}_{n+1}\boldsymbol{\phi}^H \bar{\mathbf{y}}\right)\right] \tag{57}$$

$$f(\bar{\mathbf{y}}|\mathbf{a}, \sigma^2, H_1) = \frac{1}{(\pi\sigma^2)^{MN_s}|\mathbf{C}^{-1}|} \times exp\left[\frac{-1}{\sigma^2}\left((\bar{\mathbf{y}} - \sum_{k=1}^{t_n} \bar{\mathbf{S}}\mathbf{a}_k)^H \boldsymbol{\phi}\mathbf{K}_{n+1}\boldsymbol{\phi}^H (\bar{\mathbf{y}} - \sum_{k=1}^{t_n} \bar{\mathbf{S}}\mathbf{a}_k)\right)\right] \tag{58}$$

Where $\bar{\mathbf{S}} = \boldsymbol{\phi}\mathbf{S}$ and n is the number of interfering nodes. The ML estimates $\hat{\mathbf{a}}$ and $\hat{\sigma}^2$ can now be obtained as discussed previously.

$$\left(\bar{\mathbf{S}}^H(\boldsymbol{\phi}\mathbf{K}_{n+1}\boldsymbol{\phi}^H)\bar{\mathbf{S}}\right)\sum_{k=1}^{t_n}\hat{\mathbf{a}}_k = \bar{\mathbf{S}}^H(\boldsymbol{\phi}\mathbf{K}_{n+1}\boldsymbol{\phi}^H)\bar{\mathbf{y}} \tag{59}$$

$$\hat{\sigma}_0^2 = \frac{1}{MN_s}\left(\bar{\mathbf{y}}^H(\boldsymbol{\phi}\mathbf{K}_{n+1}\boldsymbol{\phi}^H)\bar{\mathbf{y}}\right) \tag{60}$$

$$\hat{\sigma}_1^2 = \frac{1}{MN_s}\left((\bar{\mathbf{y}} - \sum_{k=1}^{t_n}\bar{\mathbf{S}}\hat{\mathbf{a}}_k)^H(\boldsymbol{\phi}\mathbf{K}_{n+1}\boldsymbol{\phi}^H)(\bar{\mathbf{y}} - \sum_{k=1}^{t_n}\bar{\mathbf{S}}\hat{\mathbf{a}}_k)\right) \tag{61}$$

Using (59-61) in (47) gives us the test statistic for the proposed target detector. To optimise the target detection procedure, we define a measurement coefficient, $\boldsymbol{\nabla}$ for the test statistic as,

$$\boldsymbol{\nabla} = (\boldsymbol{\phi}\mathbf{K}_{n+1}\boldsymbol{\phi}^H)\bar{\mathbf{S}}\left(\bar{\mathbf{S}}^H(\boldsymbol{\phi}\mathbf{K}_{n+1}\boldsymbol{\phi}^H)\bar{\mathbf{S}}\right)^{-1}\bar{\mathbf{S}}^H(\boldsymbol{\phi}\mathbf{K}_{n+1}\boldsymbol{\phi}^H) \tag{62}$$

Therefore the optimised test statistic, $\mathbb{T}$,for the proposed target detector is expressed as,

$$\mathbb{T} = \left(\frac{\bar{\mathbf{y}}^H \boldsymbol{\chi}_0 \bar{\mathbf{y}}}{\bar{\mathbf{y}}^H \boldsymbol{\chi}_1 \bar{\mathbf{y}}}\right) \underset{H_0}{\overset{H_1}{\gtrless}} \sqrt[N_y N_s]{\gamma} \tag{63}$$

Here, $\boldsymbol{\chi}_0$ and $\boldsymbol{\chi}_1$ are test statistic coefficients given by,

$$\boldsymbol{\chi}_0 = \boldsymbol{\phi}\mathbf{K}_{n+1}\boldsymbol{\phi}^H \tag{64}$$

$$\boldsymbol{\chi}_1 = \boldsymbol{\chi}_0 - 2\boldsymbol{\nabla} + \boldsymbol{\nabla}(\boldsymbol{\phi}\mathbf{K}_{n+1}\boldsymbol{\phi}^H)^{-1}\boldsymbol{\nabla} \tag{65}$$

VI. WAVEFORM SELECTION

To meet the power constraints, the sensor nodes transmit short, low power (mW) electromagnetic pulses into the sensing region and attempt to detect the reflected echoes from the target. The choice of an appropriate transmit waveform is an important design parameter for RF sensing based surveillance applications of IoT. To achieve longevity, optimum choice of a transmit waveform within IoT must fulfil the necessary criterion to achieve the desired target detection reliability while operating within the constraints of the available resources. Brevity of the transmit pulses is required to reduce the transmission costs. To reduce the signal processing complexities, the choice of a transmit waveform with good correlation properties is desirable. Gaussian and Monocycle pulses are the most commonly discussed UWB waveforms. Due to simplicity and ease of generation, they can be used within IoT with very low computational cost. However, within a large sensing region with multiple transmitting nodes, a degree of diversity in the choice of transmit waveforms among the transmitting nodes is desirable. Waveforms based on orthogonal Gegenbauer and Hermite polynomials are discussed in [39]–[42]. Waveforms generated using modified Gegenbauer functions and Hermite functions could be used to produce ultra-short RF pulses and allow multiple access. They are also less complex compared to conventional multiple access communication systems.

Modified Gegenbauer polynomials are defined in the interval [-1,1]. The recurrence relation for the n^{th} order modified Gegenbauer polynomial is written as,

$$\begin{aligned}G_n(\beta, t) &= (1-t^2)^{\frac{2\beta-1}{4}}\left(\frac{2(n+\beta-1)}{n}tG_{n-1}(\beta,t) - \frac{(n+2\beta-2)}{n}G_{n-2}(\beta,t)\right) \quad n \neq 0 \\ G_0(t) &= 1\end{aligned} \tag{66}$$

Where n is the order of the Gegenbauer polynomial and β is the shape parameter and usually $\beta > \frac{-1}{2}$. Modified Hermite polynomials are defined in the interval $[-\infty, \infty]$. n^{th} order modified Hermite polynomial is written as,

$$Hm_n(t) = e^{\frac{-t^2}{4}}(-1)^n e^{\frac{t^2}{2}} \frac{d^n}{dt^n}(e^{\frac{-t^2}{2}}) \quad n \neq 0 \qquad (67)$$
$$Hm_0(t) = 1$$

The transmit waveforms discussed in this section are easy to generate and does not require complex transmitting devices. They also provide diversity within the choice of transmit waveforms. However, due to event driven nature of IoT and spatial displacement of the sensor nodes, orthogonal waveforms do not provide a generalised solution to optimise the target detection reliability. The necessary criteria for optimum choice of the transmit waveform is the ability to make a clear distinction between its presence and absence within the received signal components. To analyse the received signal properties, hypothesis H_0 and H_1 in (16) are elaborated as,

$$H_0 : \begin{cases} H_{00}: & \mathbf{y}(n) = \mathbf{w}(n) \\ H_{01}: & \mathbf{y}(n) = \mathbf{Bh}(n) + \mathbf{n}(n) \end{cases} \qquad (68)$$

$$H_1 : \begin{cases} H_{10}: & \mathbf{y}(n) = \mathbf{As}(n) + \mathbf{n}(n) \\ H_{11}: & \mathbf{y}(n) = \mathbf{As}(n) + \mathbf{Bh}(n) + \mathbf{w}(n) \end{cases} \qquad (69)$$

Where $\mathbf{A}$ and $\mathbf{B}$ are the convolution matrices for target and interfering signal impulse responses and can be expressed as shown in (4) and (5) respectively. (68) and (69) represent possible received signal models under hypothesis H_0 and H_1 which are characterised by existence and absence of the target and the interfering waveforms. For a matched filter impulse response $\mathbf{f}$, a reliable decision regarding the existence or absence of a target can be made when the matched filter outputs under hypothesis H_0 and H_1 are clearly distinguishable. To measure the ability of the matched filter to make this distinction, we define Ease of Detection Index (δ) in (70), as shown at the bottom of this page, which is measured at 3dB SIR. Here $\star$ represents correlation operator. When the sensing conditions are known, the transmit waveform which maximises δ gives optimum reliability among the available choice of transmit waveforms. Within resource constrained IoT, the transmit power has a significant impact on the lifetime of the sensor nodes. The choice of transmit waveform while achieving high δ, must also be energy efficient to ensure longevity of the sensor nodes. The amount of transmit power required to guarantee a desired SIR at the receiver is related to various factors such as prorogation losses, target impulse response, target range, etc. For a given set of sensing conditions, the energy efficiency of the transmit waveform is defined by the Energy Efficiency Index (η). η is the ratio of the amount of transmit power (P_{Tm}) required to guarantee a desired SIR at the matched filter output to the amount of transmit power (P_{Tr}) required to guarantee the desired SIR at the sensor node receiver which is given as,

$$\eta = \frac{P_{Tm}}{P_{Tr}} = \frac{max(\mathbf{f}^H \star \mathbf{Bh})(\mathbf{As})^H(\mathbf{As})}{max(\mathbf{f}^H \star \mathbf{As})(\mathbf{Bh})^H(\mathbf{Bh})} \qquad (71)$$

η denotes the factor by which the transmit power may be reduced while ensuring desired SIR at the matched filter output. The transmit waveform which provides optimal balance between δ and η is chosen based on the criterion given by the ratio δ/η. Therefore, for a given set of sensing conditions the transmit waveform which maximises δ/η optimises the target detection reliability of IoT. When a Monocycle pulse is assumed to be the interfering waveform, δ and η of the waveforms discussed in this section are summarised in Table 1. It can be observed that for the given sensing conditions, G_4 and Hm_4 waveforms generated high δ/η ratios compared to the other waveforms. Similarly, δ/η ratio of Hm_1 waveform is less than zero which indicates that Hm_1 waveform is unsuitable for transmission. In Fig. 4 and Fig. 5, the matched filter outputs of the received signal models under hypothesis H_0 and H_1 with transmit waveforms being G_4 and Hm_1 respectively are plotted. The transmission periods of individual sensor nodes within IoT are assumed to be unsynchronised. The matched filter outputs for all 4 cases of received signal models in (68) and (69) are plotted. H_{00} indicates the received signal model under hypothesis H_0 where the target and interfering waveforms are absent. Similarly, H_{01} refers to the received signal under hypothesis H_0 in the presence of interfering waveform. Similarly, H_{10} and H_{11} refer to the received signal models under hypothesis H_1 in the absence and presence of interfering waveform. From the

TABLE 1. Comparison of Gaussian and Monocycle pulses autocorrelation functions.

Waveform	δ	η	(δ/η)
Gaussian Pulse	0.4553	0.2277	1.9995
G_0	0.4045	0.2214	1.8272
G_1	0.3906	0.3789	1.0309
G_2	0.0357	0.5609	0.0636
G_3	0.4180	0.1440	2.9024
G_4	1.2945	0.0843	15.3645
Hm_0	0.1969	0.4029	0.4888
Hm_1	-0.0333	1.3813	-0.0241
Hm_2	0.3603	0.2523	1.4281
Hm_3	1.2444	0.0958	12.9957
Hm_4	1.2675	0.0857	14.7904

$$\delta = \frac{(max(\mathbf{f}^H \star \mathbf{As}) - max(\mathbf{f}^H \star \mathbf{Bh}))(max(\mathbf{f}^H \star (\mathbf{As} + \mathbf{Bh})) - max(\mathbf{f}^H \star \mathbf{Bh}))}{max(\mathbf{f}^H \star \mathbf{Bh})} \qquad (70)$$

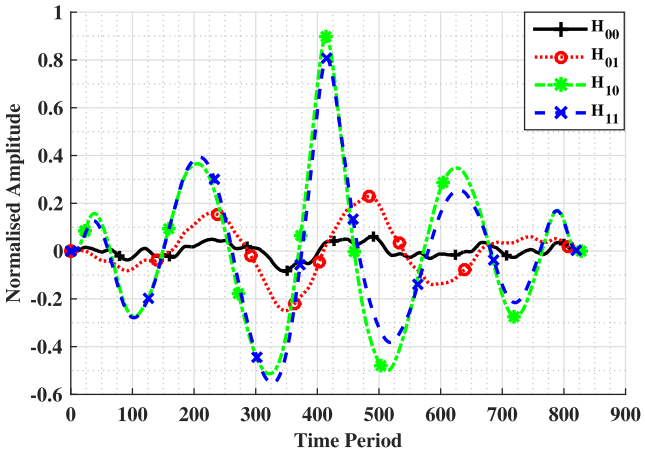

FIGURE 4. Matched filter output for G_4 transmit waveform and interfering Monocycle pulse.

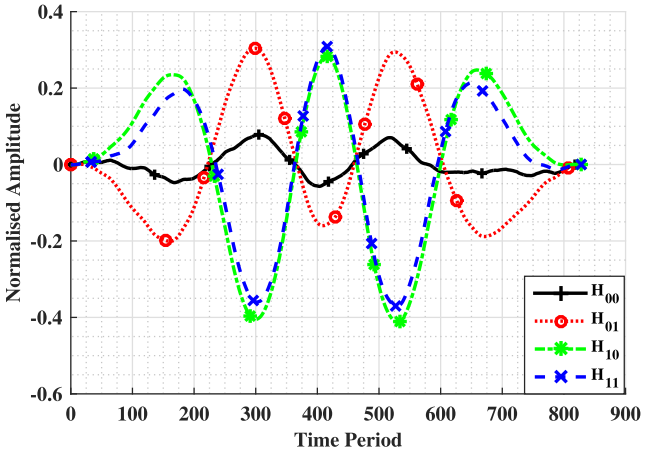

FIGURE 5. Matched filter output for Hm_1 transmit waveform and interfering Monocycle pulse.

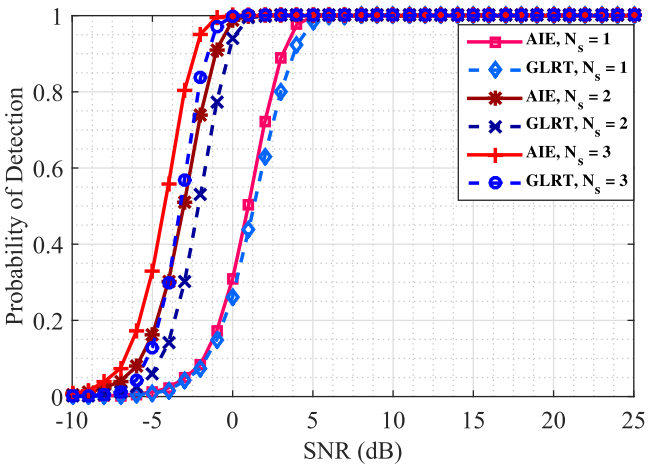

FIGURE 6. Target detection performance of the proposed AIE detector vs conventional GLRT detector in the presence of interference at SIR = 3dB.

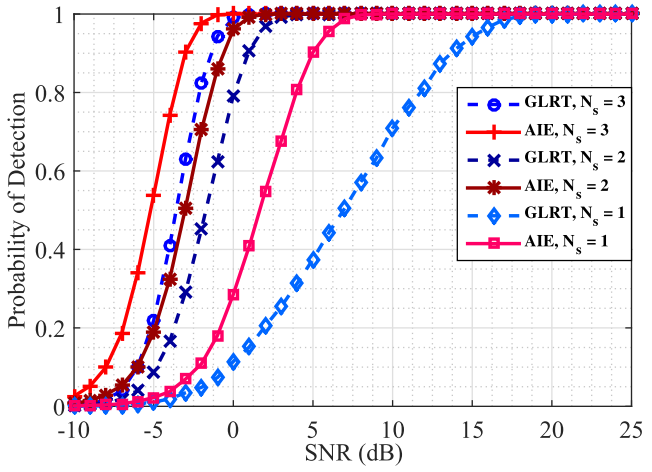

FIGURE 7. Target detection performance of the proposed AIE detector vs conventional GLRT detector in the presence of interference at SIR = −3dB.

plots, it can be observed that, when G_4 waveform is transmitted, a clear distinction existed between matched filter outputs under hypothesis H_0 and H_1 which indicates greater detection reliability. However, when Hm_1 waveform is transmitted, no distinction between matched filter outputs under hypothesis H_0 and H_1 can be observed which indicates an uncertainty in the decision-making process. Hence, optimum choice of the transmit waveforms among the neighbouring clusters can be made by analysing the δ/η ratio of the available waveforms under the give set of sensing conditions.

VII. PERFORMANCE ANALYSIS

In this section, we demonstrate the target detection performance of the proposed target detector for IoT in the presence of interference and clutter. Target detection performance is quantised in terms of Probability of Detection (P_d) and Probability of False alarm (P_{fa}). P_d is defined as the ability of the target detector to accurately make a decision regarding the existence of a target within the sensing region. P_{fa} is the rate at which the target detector makes a faulty decision in the absence of a target. Here we consider IoT where the clusters of transmitting and receiving nodes are deployed within the sensing region with each cluster accounting for surveillance within its range. Each cluster is assumed to consist of a transmitting primary node, which is referred to as a control centre and receiving nodes. We show through simulation results that having multiple receiving nodes within each cluster increases the reliability with which the presence of targets can be detected. For simulations, we consider moderate and aggressive sensor node deployment strategies. In a moderate deployment strategy, the individual clusters are widely spaced and the interference caused by the neighbouring clusters is relatively low. However, this is achieved as a trade-off with the target detection reliability as this strategy results in poor coverage within the sensing region and hence may lead to increased miss detections. In aggressive deployment strategy, while better coverage within the sensing region maybe ensured, however the sensor nodes experience increased interference from the neighbouring clusters. We also consider

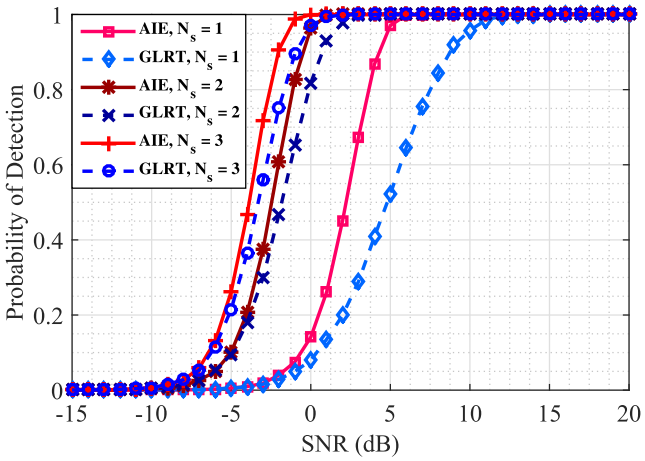

FIGURE 8. Target detection performance of the proposed AIE detector in the presence of clutter at SCR = 3dB.

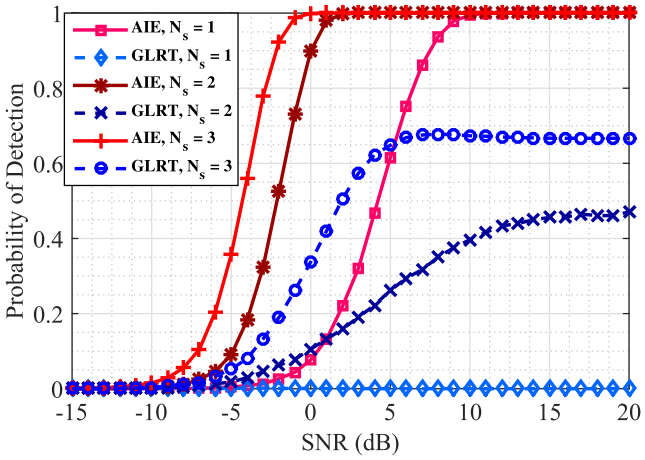

FIGURE 9. Target detection performance of the proposed AIE detector in the presence of clutter at SCR = −3dB.

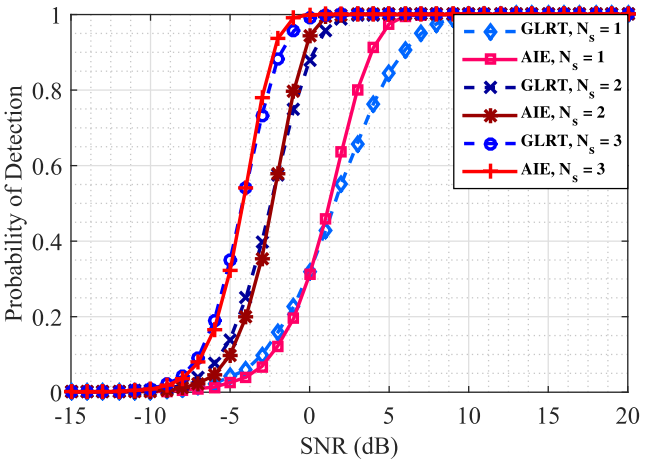

FIGURE 10. Target detection performance of the proposed AIE detector vs conventional GLRT detector in the presence of interference and clutter at SIR = 3dB and SCR = 3dB.

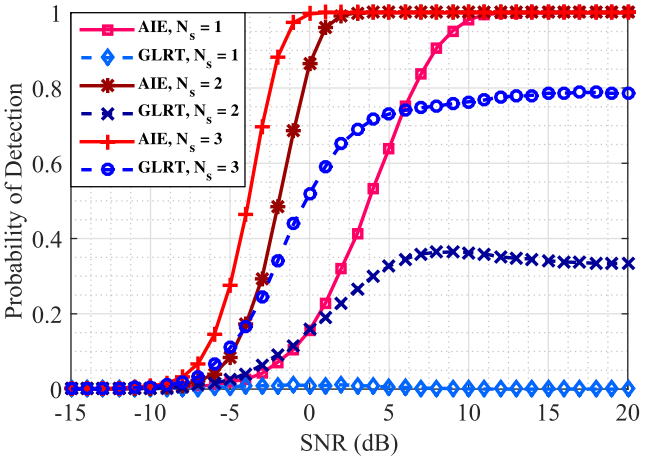

FIGURE 11. Target detection performance of the proposed AIE detector vs conventional GLRT detector in the presence of interference and clutter at SIR = 3dB and SCR = −3dB.

the presence of a cluttered background environment. Existing threshold based detection strategies for IoT fail to provide reliable target detection performance in the presence of clutter. We show that our proposed target detector provides a more reliable target detection performance in the presence of clutter. We compare the target detection performance of the proposed target detector with a simple GLRT detector under similar sensing conditions. For simulations, we resort to Monte-Carlo techniques and thresholds are evaluated to ensure required maximum false alarm rate by resorting to $100/P_{fa}$ independent simulations. Acceptable false alarm rate is assumed to be 10^{-4}. The length N_t of the transmit signal vector $\mathbf{s}$ is assumed to be 32 samples within each cluster and N_a is assumed to be 4. Due to cooperative nature of IoT, the control centre is assumed to have the knowledge of the transmit waveforms from the neighbouring sensor nodes which contribute to interference. However due to spatial displacement of the sensor nodes, the phase of the interfering waveform is assumed to be unknown. We analyse the target detection performances for three different scenarios related to the sensing conditions. In case1, we simulate the target detection performance of the proposed target detector in the presence of interference and clutter respectively and compare its performance with that of a GLRT detector in each scenario. In case2, we consider a harsh sensing environment with both clutter and interference being present. In case3, we analyse the performance of the proposed detector with compressive sensing and its effect on target detection reliability.

Case 1: In this case, the performances of the proposed detector are analysed in the presence of interference and clutter respectively. In Fig. 6 the target detection performances of the proposed Adaptive Interference Estimator (AIE) and GLRT detectors in the presence of interference and absence of clutter are shown. Results are simulated for the case of 1,2 and 3 receiving sensor nodes. Signal to Interference Ratio (SIR) is assumed to be 3dB and the interfering waveform is assumed to be G4. SIR at the detector is

TABLE 2. Performance analysis of the proposed detector in case 1.

SIR/SCR (dB)	Receiving Nodes	SNR at 100% P_d		Performance Gain	SNR at 80% P_d		Performance Gain
		AIE	GLRT		AIE	GLRT	
SIR = 3dB	$N_s = 1$	5.9dB	7dB	1.1dB	2.5dB	3dB	0.5dB
	$N_s = 2$	1.7dB	2.8dB	1.1dB	-1.6dB	-0.8dB	0.8dB
	$N_s = 3$	-0.1dB	1dB	1dB	-3.2dB	-2.2dB	0.8dB
SIR = -3dB	$N_s = 1$	9.1dB	21.1dB	12dB	3.9dB	11.8dB	7.9dB
	$N_s = 2$	3dB	5dB	2dB	-1.4dB	0.2dB	1.6dB
	$N_s = 3$	0dB	2dB	2dB	-3dB	-2.2dB	1.4dB
SCR = 3dB	$N_s = 1$	6dB	11dB	5dB	2.6dB	5 dB	2.4dB
	$N_s = 2$	1.5dB	4.8dB	3.3dB	-1.6dB	-0.7dB	0.9dB
	$N_s = 3$	0dB	1.9dB	1.9dB	-3.2dB	-2.7dB	0.5dB
SCR = -3dB	$N_s = 1$	12dB	N/A	N/A	6.4dB	N/A	N/A
	$N_s = 2$	3dB	N/A	N/A	-0.6dB	N/A	N/A
	$N_s = 3$	0.3dB	N/A	N/A	-2.9dB	10.8dB	13.7dB

TABLE 3. Performance analysis of the proposed detector in case 2.

Disturmance (dB)	Receiving Nodes	SNR at 100% P_d		Performance Gain	SNR at 80% P_d		Performance Gain
		AIE	GLRT		AIE	GLRT	
[SIR SCR] = [3 3]dB	$N_s = 1$	7.9dB	13.8dB	5.9dB	3dB	5.9dB	2.9dB
	$N_s = 2$	2.9dB	5dB	2.1dB	-1dB	-0.6dB	0.4dB
	$N_s = 3$	0.6dB	2.2dB	1.6dB	-2.9dB	-2.4dB	0.58dB
[SIR SCR] = [3 -3]dB	$N_s = 1$	13.5dB	N/A	N/A	6.7dB	N/A	N/A
	$N_s = 2$	3.9dB	N/A	N/A	-0.3dB	N/A	N/A
	$N_s = 3$	1dB	N/A	N/A	-2.4dB	N/A	N/A
[SIR SCR] = [-3 3]dB	$N_s = 1$	11.1dB	N/A	N/A	4.9dB	N/A	N/A
	$N_s = 2$	4dB	7.7dB	3.7dB	-0.7dB	0.7dB	1.4dB
	$N_s = 3$	2.5dB	6dB	3.5dB	-1.8dB	-0.5dB	0.3dB

measured as,

$$SIR = \frac{\|\mathbf{Sa}\|^2}{\|\sum_{k=1}^{b_n} \mathbf{H}_k b_k\|^2} \tag{72}$$

This is a relatively moderate sensing environment in the absence clutter. The test statistic for AIE detector defined in (62)-(65) can be modified for this scenario as,

$$\mathbb{T} = \left(\frac{\mathbf{y}^H \boldsymbol{\chi}_0 \mathbf{y}}{\mathbf{y}^H \boldsymbol{\chi}_1 \mathbf{y}}\right) \underset{H_0}{\overset{H_1}{\gtrless}} \sqrt[N_y N_s]{\gamma} \tag{73}$$

Where χ_1 and χ_2 are test statistic coefficients given in (64) and (65). The new measurement coefficients for this case are,

$$\mathbf{K}_j = \left(\prod_{l=1}^{j} \mathbf{M}_{l-1}\right)^H \left(\prod_{l=1}^{j} \mathbf{M}_{l-1}\right) \tag{74}$$

$$\mathbf{M}_n = \mathbf{I} - \mathbf{H}_n \mathbf{R}_{\mathbf{h}nn}^{-1} \mathbf{H}_n^H \mathbf{K}_n \quad \text{n}\neq 0 \tag{75}$$

$$\mathbf{M}_0 = \mathbf{I} \tag{76}$$

In moderate sensing conditions with low interfering signal strengths, the target detection performances of the proposed AIE detector and GLRT detector are nearly identical with AIE detector slightly outperforming the GLRT detector. In Fig. 7, the performances of AIE and GLRT detectors are compared in relatively harsher sensing environment at SIR = -3dB. Under harsher sensing conditions, the proposed AIE detector significantly outperformed the conventional GLRT detector. In Table 2 target detection performances of AIE and GLRT detectors are summarised. It has been observed that deploying additional receiving nodes within the sensing region increases the efficiency of the target detector. However, beyond a certain upper threshold any additional receiving nodes yield no significant performance gain.

Similarly, in In Fig. 8 and Fig. 9 we show the performances of AIE and GLRT detectors in the presence of clutter with Signal to Clutter Ratio (SCR) of 3dB and -3dB respectively. While the GLRT detector experienced a severe deterioration

TABLE 4. Performance analysis of the proposed detector in case 3 at 40% compression.

SNR	N_s	Probability of Detection (P_d)		Tradeoff	Probability of Detection (P_d)		Tradeoff
		GLRT	C-GLRT		AIE	C-AIE	
0	1	0.3200	0.0102	0.3098	0.3112	0.0441	0.2671
	2	0.8794	0.0436	0.8358	0.9434	0.1808	0.7626
	3	0.9913	0.3602	0.6311	0.9997	0.5927	0.4070
5	1	0.8463	0.0250	0.8213	0.9754	0.1543	0.8211
	2	1	0.2317	0.7683	1	0.7673	0.2327
	3	1	0.8850	0.1150	1	0.9985	0.0015
10	1	0.9973	0.0256	0.9717	1	0.3138	0.6862
	2	1	0.4351	0.5649	1	0.9975	0.0025
	3	1	0.9970	0.0030	1	1	0
15	1	1	0.0103	0.9897	1	0.4920	0.5080
	2	1	0.5185	0.4815	1	1	0
	3	1	1	0	1	1	0

TABLE 5. Performance analysis of the proposed detector in case 3 at 60% compression.

SNR	N_s	Probability of Detection (P_d)		Tradeoff	Probability of Detection (P_d)		Tradeoff
		GLRT	C-GLRT		AIE	C-AIE	
0	1	0.3200	0.0035	0.3165	0.3112	0.0096	0.3016
	2	0.8794	0.0152	0.8642	0.9434	0.0554	0.8880
	3	0.9913	0.0958	0.8955	0.9997	0.2043	0.7954
5	1	0.8463	0.0038	0.8605	0.9754	0.0291	0.9535
	2	1	0.0692	0.9308	1	0.2724	0.7276
	3	1	0.4996	0.5004	1	0.8059	0.1941
10	1	0.9973	0.0030	0.9943	1	0.0305	0.9695
	2	1	0.1344	0.8656	1	0.5750	0.4250
	3	1	0.8253	0.1747	1	0.9969	0.0031
15	1	1	0.0035	0.9965	1	0.0124	0.9876
	2	1	0.1448	0.8552	1	0.7646	0.2354
	3	1	0.9319	0.0681	1	1	0

in the target detection performance in the presence of clutter, the target detection performance of the proposed AIE detector remained robust. In Fig. 9 it can be seen that in the presence of strong clutter, the GLRT detector completely failed to provide reliable detection performance while the proposed detector showed robust performance. This clearly validates the significance of the clutter projection matrix in (15) to achieve increased target detection performance. A detailed comparison of AIE and GLRT detectors in the presence of clutter is summarised in Table 2.

Case 2: Here, we simulate a sensing environment which consists of clutter and interference to analyse the performance of the proposed target detector. In Fig. 10, we considered the presence of relatively weak clutter and interfering signals and the target detection performances of AIE and GLRT detectors are compared. Similarly, in Fig. 11 and Fig. 12 we compare the target detection performances of AIE and GLRT detectors in the presence of strong clutter and interference respectively. GLRT detector failed to achieve reliable detection rates in harsh sensing conditions and the proposed AIE detector outperformed the GLRT detector by a significant margin. The performance evaluations in this case are summarised in Table. 3. In Fig. 13 and Fig. 14 the performance of the proposed detector in the presence of multiple interfering

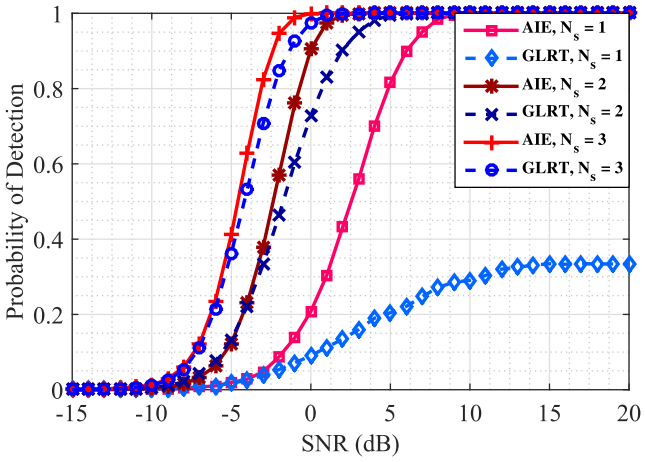

FIGURE 12. Target detection performance of the proposed AIE detector vs conventional GLRT detector in the presence of interference and clutter at SIR = −3dB and SCR = 3dB.

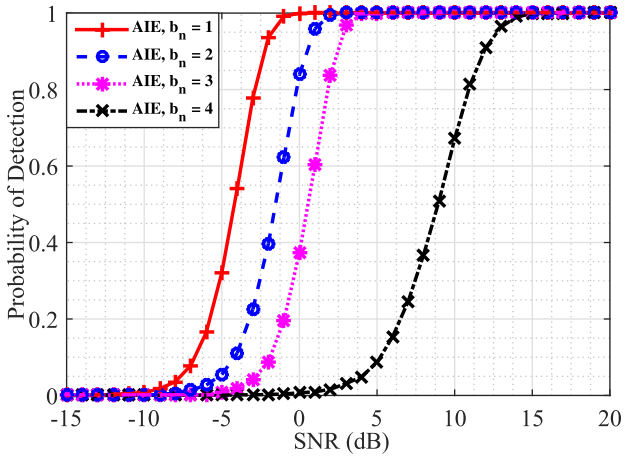

FIGURE 13. Target detection performance of the proposed AIE detector in the presence of multiple interfering nodes and 3 receiving nodes at SIR = 3dB and SCR = 3dB.

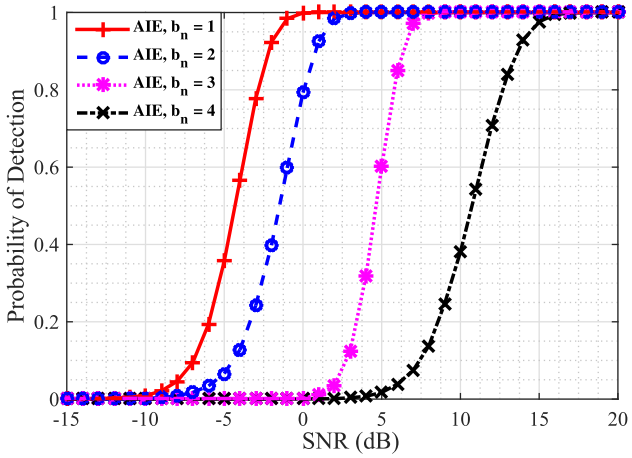

FIGURE 14. Target detection performance of the proposed AIE detector in the presence of multiple interfering nodes and 3 receiving nodes at SIR = −3dB and SCR = 3dB.

nodes is shown. From the simulation results, performance deterioration with increasing number of interfering nodes can be observed. This has occurred due to unknown phase of the interfering waveforms.

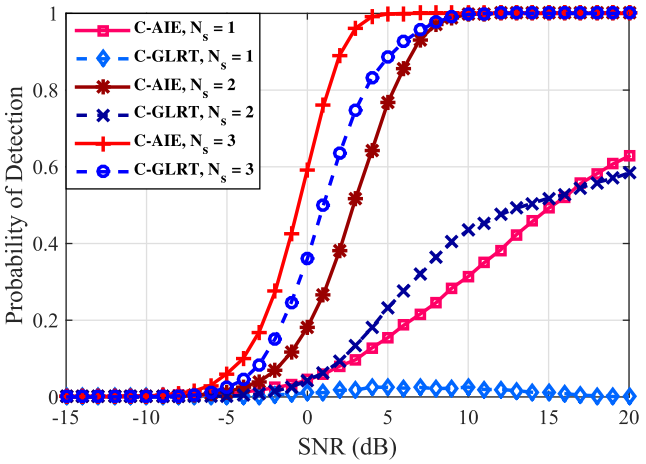

FIGURE 15. Target detection performance of the proposed AIE detector vs conventional GLRT detector using compressive sampling in the presence of interference and clutter at SIR = 3dB and SCR = 3dB and 40 percent compression.

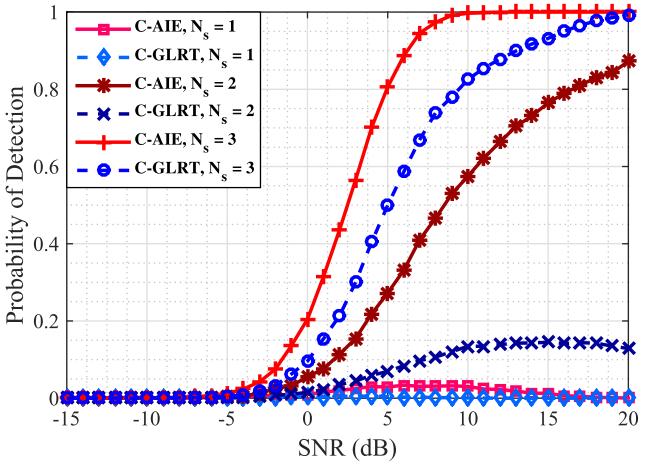

FIGURE 16. Target detection performance of the proposed AIE detector vs conventional GLRT detector using compressive sampling in the presence of interference and clutter at SIR = 3dB and SCR = 3dB and 60 percent compression.

Case 3: Within resource constrained IoT, the sensor nodes are expected to operate independently with limited available power. The lifetime of the sensor nodes is of utmost importance to ensure longevity of the IoT. It has already been established in the existing literature that a major share of the available power is consumed during data transmission between the sensor nodes and the control centre. Transmitting compressed received signal samples to the control centre is observed to be a potential solution to reduce the power consumption. However, data compression is achieved as a trade-off with the target detection reliability. Here we investigate the performance of the proposed target detector using compressed received signal samples.

In Fig. 15 we show the target detection performances of the AIE and GLRT detectors using compressed received signal samples at 40% compression and the results are summarised in Table. 4. The amount of detection performance loss which occurred due to compression is also shown in Table. 4.

Similarly in Fig. 16 performances of the AIE and GLRT detectors are compared at 60% compression and corresponding summary of detection performances are shown in Table. 5. It can be observed from the simulation results that by adjusting the compression ratio adaptively with respect to the changes in the sensing conditions, compressive sensing can be implemented without any significant loss in the target detection performance.

VIII. CONCLUSION

In this paper, RF sensing based surveillance applications of IoT have been addressed. An energy efficient target detection architecture, which is suitable for resource constrained IoT has been proposed. The sensing environments in which IoT are expected to operate have been considered while deriving the received signal models and the corresponding pdfs. We proposed a two-step detection model to optimise the energy efficiency and detection reliability of the target detector. The proposed two-step detection scheme, while reducing the computational burden also reduces the decision-making time. Our proposed target detection model estimates the interfering signal strengths from each interfering node, which allows the sensor nodes to dynamically adopt to changes in interfering waveforms from the neighbouring clusters while providing reliable target detection performance. To reduce the transmission costs, we addressed compressive sensing scheme where the sensor nodes are only required to transmit compressed received signal samples to the control centre. We have shown through simulations results that under suitable sensing conditions compressive sensing can be used without any significant loss in target detection reliability.

Future Work: In our proposed target detection architecture, the control centre gathers the received data from all the sensor nodes within its cluster to make a decision regarding the existence or absence of a target. Using a simple low-complexity target detector at the individual sensor nodes may be considered where the sensor nodes are capable of making a preliminary decision before transmitting the data to the control centre. This reduces the frequency of data exchange between the sensor nodes and the control centre thereby increasing the lifetime of the IoT. While the proposed target detector provides reliable target detection rates, authors consider addressing the unknown parameter estimation procedure in the future work to achieve more reliable target detection rates.

APPENDIX
INVERSE OF DISTURBANCE COVARIANCE MATRIX

Given $\mathbf{R}_d$ in (11), in this section we discuss the procedure to estimate $\mathbf{R}_d^{-1}$. From (12), it can be observed that $\mathbf{R}_d^{-1}$ can be obtained by estimating the inverse of $(\varsigma\boldsymbol{\lambda}_c+\sigma^2\mathbf{I})^{-1}$. Here $\sigma^2\mathbf{I}$ is a full rank matrix and $\varsigma\boldsymbol{\lambda}_c$ is a diagonal matrix of rank r i.e., $\varsigma\boldsymbol{\lambda}_c$ can only have up to r non zero elements. Following results from [38], the matrix $\varsigma\boldsymbol{\lambda}_c$ can be decomposed into a sum of matrices of rank one i.e.,

$$\begin{aligned}\varsigma\boldsymbol{\lambda}_c &= \sum_{k=1}^{r}\boldsymbol{\delta}_k \\ \boldsymbol{\delta}_i\boldsymbol{\delta}_j &= 0_{M\times M} \quad i\neq j\end{aligned} \tag{77}$$

Here, $\boldsymbol{\delta}_k$ is a null matrix where only the k^{th} diagonal element is non-zero and the rank of $\boldsymbol{\delta}_k$ is one. The solution to $(\sigma^2\mathbf{I}+\varsigma\boldsymbol{\lambda}_c)^{-1}$ can be obtained by solving (13) recursively. Based on the initial conditions of (13), the first order recursive inverse coefficients can be obtained as,

$$\begin{aligned}\boldsymbol{\kappa}_1^{-1} &= \sigma^{-2}\mathbf{I} \\ v_1 &= \frac{1}{1+trace(\boldsymbol{\kappa}_1^{-1}\boldsymbol{\delta}_1)}\end{aligned} \tag{78}$$

Since, $\boldsymbol{\delta}_1$ is a diagonal matrix with only one non-zero diagonal element which is λ_{c1}, $trace(\boldsymbol{\kappa}_1^{-1}\boldsymbol{\delta}_1)=\lambda_{c1}/\sigma^2$. Therefore, the first order recursive inverse coefficient can be written as,

$$v_1 = \frac{\sigma^2}{\sigma^2+\lambda_{c1}} \tag{79}$$

Substituting (79) in (13), the second order recursive inverse coefficients are obtained as,

$$\begin{aligned}\boldsymbol{\kappa}_2^{-1} &= \boldsymbol{\kappa}_1^{-1} - v_1\boldsymbol{\kappa}_1^{-1}\boldsymbol{\delta}_1\boldsymbol{\kappa}_1^{-1} \\ &= \sigma^{-2}\mathbf{I} - \frac{\sigma^{-2}}{\sigma^2+\lambda_{c1}}\boldsymbol{\delta}_1 \\ &= \sigma^{-2}\left(\mathbf{I}-\frac{\boldsymbol{\delta}_1}{\sigma^2+\lambda_{c1}}\right) \\ v_2 &= \frac{1}{1+trace(\boldsymbol{\kappa}_2^{-1}\boldsymbol{\delta}_2)} \\ &= \frac{1}{1+trace\left(\sigma^{-2}\left(\mathbf{I}-\frac{\boldsymbol{\delta}_1}{\sigma^2+\lambda_{c1}}\right)\boldsymbol{\delta}_2\right)}\end{aligned} \tag{80}$$

From (77), it may be recalled that $\delta_1\delta_2$ is a null matrix. Therefore, the second order recursive coefficient, v_2 can be obtained as,

$$\begin{aligned}v_2 &= \frac{1}{1+trace(\sigma^{-2}\boldsymbol{\delta}_2)} \\ &= \frac{\sigma^2}{\sigma^2+\lambda_{c2}}\end{aligned} \tag{81}$$

Similarly, from (80) and (81), the third order recursive inverse coefficients are obtained as,

$$\begin{aligned}\boldsymbol{\kappa}_3^{-1} = \sigma^{-2}&\left(\mathbf{I}-\frac{\boldsymbol{\delta}_1}{\sigma^2+\lambda_{c1}}\right) - \frac{\sigma^2}{\sigma^2+\lambda_{c2}}\sigma^{-2} \\ &\times\left(\mathbf{I}-\frac{\boldsymbol{\delta}_1}{\sigma^2+\lambda_{c1}}\right)\boldsymbol{\delta}_2\sigma^{-2}\left(\mathbf{I}-\frac{\boldsymbol{\delta}_1}{\sigma^2+\lambda_{c1}}\right)\end{aligned} \tag{82}$$

As mentioned previously in (77), since $\boldsymbol{\delta}_i\boldsymbol{\delta}_j = \mathbf{0}_{N_c\times N_c}$ when $i\neq j$, (82) can be simplified as,

$$\kappa_3^{-1} = \sigma^{-2}\left(\mathbf{I}-\frac{\boldsymbol{\delta}_1}{\sigma^2+\lambda_{c1}}-\frac{\boldsymbol{\delta}_2}{\sigma^2+\lambda_{c2}}\right) \tag{83}$$

To obtain $(\varsigma\boldsymbol{\lambda}_c+\sigma^2\mathbf{I})^{-1}$, $(r+1)^{th}$ order recursive inverse coefficients are required. Observing Equations (83,80,78) and using the principle of induction, the $(r+1)^{th}$ order recursive inverse coefficient can be obtained which gives the solution to $(\varsigma\boldsymbol{\lambda}_c+\sigma^2\mathbf{I})^{-1}$ which is,

$$(\sigma^2\mathbf{I}+\varsigma\boldsymbol{\lambda}_c)^{-1}=\sigma^{-2}\left(\mathbf{I}-\frac{\boldsymbol{\delta}_1}{\sigma^2+\lambda_{c1}}-\frac{\boldsymbol{\delta}_2}{\sigma^2+\lambda_{c2}}\cdots-\frac{\boldsymbol{\delta}_r}{\sigma^2+\lambda_{cr}}\right) \quad (84)$$

Substituting (84) in (12), $\mathbf{R}_d^{-1}$ can be written as,

$$\mathbf{R}_d^{-1}=\sigma^{-2}\boldsymbol{\Phi}_d\times\left(\mathbf{I}-\frac{\boldsymbol{\delta}_1}{\sigma^2+\lambda_{c1}}-\frac{\boldsymbol{\delta}_2}{\sigma^2+\lambda_{c2}}\cdots-\frac{\boldsymbol{\delta}_r}{\sigma^2+\lambda_{cr}}\right)\boldsymbol{\Phi}_d^H \quad (85)$$

Usually the clutter returns are significantly stronger than noise power at the sensing nodes. Under such scenarios, the following approximation can be made; $\sigma^2+\lambda_{ci}\approx\lambda_{ci}$. Since $\boldsymbol{\Phi}_d\boldsymbol{\Phi}_d^H=\mathbf{I}$, (85) can be rewritten as,

$$\mathbf{R}_d^{-1}=\sigma^{-2}\left(\mathbf{I}-\sum_{i=1}^{r}\boldsymbol{\Phi}_{di}\boldsymbol{\Phi}_{di}^H\right) \quad (86)$$

REFERENCES

[1] D. Estrin, R. Govindan, J. Heidemann, and S. Kumar, "Next century challenges: Scalable coordination in sensor networks," in *Proc. 5th Annu. ACM/IEEE Int. Conf. Mobile comput. Netw.*, 1999, pp. 263–270.
[2] A. Arora *et al.*, "A line in the sand: A wireless sensor network for target detection, classification, and tracking," *Comput. Netw.*, vol. 46, no. 5, pp. 605–634, 2004.
[3] M. Ali, A. Böhm, and M. Jonsson, "Wireless sensor networks for surveillance applications—A comparative survey of MAC protocols," in *Proc. 4th Int. Conf. Wireless Mobile Commun.*, Jul. 2008, pp. 399–403.
[4] F. T. Jaigirdar and M. M. Islam, "A new cost-effective approach for battlefield surveillance in wireless sensor networks," in *Proc. Int. Conf. Netw. Syst. Secur. (NSysS)*, Jan. 2016, pp. 1–6.
[5] F. T. Jaigirdar, M. M. Islam, and S. R. Huq, "An efficient and cost effective maximum clique analysis based approximation in military application of wireless sensor network," in *Proc. 14th Int. Conf. Comput. Inf. Technol.*, Dec. 2011, pp. 85–90.
[6] P. K. Dutta, A. K. Arora, and S. B. Bibyk, "Towards radar-enabled sensor networks," in *Proc. 5th Int. Conf. Inf. Process. Sensor Netw.*, Apr. 2006, pp. 467–474.
[7] M. Ditzel and F. H. Elferink, "Low-power radar for wireless sensor networks," in *Proc. Eur. Radar Conf.*, Sep. 2006, pp. 139–141.
[8] R. Kozma *et al.*, "A radar-enabled collaborative sensor network integrating cots technology for surveillance and tracking," *Sensors*, vol. 12, no. 2, p. 1336, 2012.
[9] S. Azevedo and T. E. McEwan, "Micropower impulse radar," *IEEE Potentials*, vol. 16, no. 2, pp. 15–20, Apr. 1997.
[10] The Samraksh Company. *User Manual for the Bumblebee: A Low-Power, Mote-Scale Pulsed Doppler Radar Sensor Board*, accessed on Oct. 10, 2016. [Online]. Available: https://samraksh.com/index.php/products/sensors/32-product-pages/products-sensors/71-bumblebee-radar
[11] S. Meguerdichian, F. Koushanfar, G. Qu, and M. Potkonjak, "Exposure in wireless ad-hoc sensor networks," in *Proc. 7th Annu. Int. Conf. Mobile Comput. Netw.*, 2001, pp. 139–150.
[12] V. Phipatanasuphorn and P. Ramanathan, "Vulnerability of sensor networks to unauthorized traversal and monitoring," *IEEE Trans. Comput.*, vol. 53, no. 3, pp. 364–369, Mar. 2004.
[13] T. He *et al.*, "Energy-efficient surveillance system using wireless sensor networks," in *Proc. 2nd Int. Conf. Mobile Syst., Appl., Services*, 2004, pp. 270–283.
[14] P. K. Varshney, *Distributed Detection and Data Fusion*, 1st ed. New York, NY, USA: Springer-Verlag, 1996.
[15] J. Liang and Q. Liang, "Design and analysis of distributed radar sensor networks," *IEEE Trans. Parallel Distrib. Syst.*, vol. 22, no. 11, pp. 1926–1933, Nov. 2011.
[16] O. Younis and S. Fahmy, "Distributed clustering in ad-hoc sensor networks: A hybrid, energy-efficient approach," in *Proc. 23rd Annu. Joint Conf. IEEE Comput. Commun. Soc. (INFOCOM)*, vol. 1. Mar. 2004, p. 640.
[17] L. Ramaswamy, B. Gedik, and L. Liu, "A distributed approach to node clustering in decentralized peer-to-peer networks," *IEEE Trans. Parallel Distrib. Syst.*, vol. 16, no. 9, pp. 814–829, Sep. 2005.
[18] C. Liu, K. Wu, Y. Xiao, and B. Sun, "Random coverage with guaranteed connectivity: Joint scheduling for wireless sensor networks," *IEEE Trans. Parallel Distrib. Syst.*, vol. 17, no. 6, pp. 562–575, Jun. 2006.
[19] S. K. Bolisetti, K. Ahmed, M. Patwary, and M. Abdel-Maguid, "Compressive parametric glrt detector for airborne mimo radar," in *Proc. Int. Conf. Wireless Commun. Signal Process. (WCSP)*, Nov. 2011, pp. 1–5.
[20] N. Pulsone and M. Zatman, "A computationally efficient two-step implementation of the GLRT," *IEEE Trans. Signal Process.*, vol. 48, no. 3, pp. 609–616, Mar. 2000.
[21] E. Conte, A. De Maio, and G. Ricci, "GLRT-based adaptive detection algorithms for range-spread targets," *IEEE Trans. Signal Process.*, vol. 49, no. 7, pp. 1336–1348, Jul. 2001.
[22] B. Liu, B. Chen, and J. Michels, "A GLRT for radar detection in the presence of compound-gaussian clutter and additive white gaussian noise," in *Proc. Workshop Sensor Array Multichannel Signal Process.*, Aug. 2002, pp. 87–91.
[23] K. Ahmed, S. Kothuri, M. Patwary, and M. Abdel-Maguid, "Subspace compressive GLRT detector for airborne MIMO radar," in *Proc. 16th Asia–Pacific Conf. Commun. (APCC)*, Nov. 2010, pp. 302–306.
[24] S. K. Bolisetti, M. Patwary, K. Ahmed, A.-H. Soliman, and M. Abdel-Maguid, "Subspace compressive GLRT detector for MIMO radar in the presence of clutter," *Sci. World J.*, vol. 2015, Aug. 2015, Art. no. 341619.
[25] N. A. Goodman, P. R. Venkata, and M. A. Neifeld, "Adaptive waveform design and sequential hypothesis testing for target recognition with active sensors," *IEEE J. Sel. Topics Signal Process.*, vol. 1, no. 1, pp. 105–113, Jun. 2007.
[26] D. A. Garren, M. K. Osborn, A. C. Odom, J. S. Goldstein, S. U. Pillai, and J. R. Guerci, "Enhanced target detection and identification via optimised radar transmission pulse shape," *IEE Proc.-Radar, Sonar Navigat.*, vol. 148, no. 3, pp. 130–138, Jun. 2001.
[27] L. P. Roy and R. V. R. Kumar, "Accurate k-distributed clutter model for scanning radar application," *IET Radar, Sonar Navigat.*, vol. 4, no. 2, pp. 158–167, Apr. 2010.
[28] R. Kelmn, *Principles of Space-Time Adaptive Processing*. Stevenage, U.K.: The Institute of Electrical Engineers, 2002.
[29] L. P. Roy and R. V. R. Kumar, "A GLRT detector in partially correlated texture based compound-Gaussian clutter," in *Proc. Nat. Conf. Commun. (NCC)*, Jan. 2010, pp. 1–5.
[30] S. Kraut, L. T. McWhorter, and L. L. Scharf, "A canonical representation for distributions of adaptive matched subspace detectors," in *Proc. Conf. Rec. 31st Asilomar Conf. Signals, Syst. Comput.*, vol. 2. Nov. 1997, pp. 1331–1335.
[31] S. Kraut and L. L. Scharf, "The CFAR adaptive subspace detector is a scale-invariant GLRT," *IEEE Trans. Signal Process.*, vol. 47, no. 9, pp. 2538–2541, Sep. 1999.
[32] S. Kraut, L. L. Scharf, and L. T. McWhorter, "Adaptive subspace detectors," *IEEE Trans. Signal Process.*, vol. 49, no. 1, pp. 1–16, Jan. 2001.
[33] L. L. Scharf and L. T. McWhorter, "Adaptive matched subspace detectors and adaptive coherence estimators," in *Proc. Conf. Rec. 13th Asilomar Conf. Signals, Syst. Comput.*, vol. 2. Nov. 1996, pp. 1114–1117.
[34] W. L. Melvin and G. A. Showman, "An approach to knowledge-aided covariance estimation," *IEEE Trans. Aerosp. Electron. Syst.*, vol. 42, no. 3, pp. 1021–1042, Jul. 2006.
[35] A. G. Jaffer, B. Himed, and P. T. Ho, "Estimation of range-dependent clutter covariance by configuration system parameter estimation," in *Proc. IEEE Int. Radar Conf.*, May 2005, pp. 596–601.
[36] E. Conte, A. D. Maio, and G. Ricci, "Covariance matrix estimation for adaptive CFAR detection in compound-Gaussian clutter," *IEEE Trans. Aerosp. Electron. Syst.*, vol. 38, no. 2, pp. 415–426, Apr. 2002.
[37] F. Gini, "Sub-optimum coherent radar detection in a mixture of K-distributed and Gaussian clutter," *IEE Proc.-Radar, Sonar Navigat.*, vol. 144, no. 1, pp. 39–48, Feb. 1997.

[38] K. S. Miller, "On the inverse of the sum of matrices," *Math. Mag.*, vol. 54, no. 2, pp. 67–72, 1981.
[39] F. Elbahhar, A. Rivenq-Menhaj, J. M. Rouvaen, M. Heddebaut, and T. Boukour, "Comparison between DS-CDMA and modified Gegenbauer functions for a multiuser communication ultra-wideband system," *Commun., IEE Proceedings-*, vol. 152, no. 6, pp. 1021–1027, Dec. 2005.
[40] L. B. Michael, M. Ghavami, and R. Kohno, "Multiple pulse generator for ultra-wideband communication using Hermite polynomial based orthogonal pulses," in *Proc. IEEE Conf. Ultra Wideband Syst. Technol.*, May 2002, pp. 47–51.
[41] L. Sakkila, A. Rivenq, C. Tatkeu, F. ElBahhar, J. Rouvaen, and Y. ElHillali, *Short Range Radar Based on UWB Technology*. Rijeka, Croatia: InTech, 2010.
[42] L. Sakkila *et al.*, "Performances of micropower UWB radar using orthogonal waveforms," *Wireless Eng. Technol.*, vol. 5, no. 3, p. 74, 2014.

SIVA KARTEEK BOLISETTI (S'17) received the B.Tech. degree in electrical and electronics engineering from V. R. Siddhartha Engineering College, India, in 2008, and the M.Sc. degree in telecommunication engineering from Staffordshire University, Stafford, U.K., in 2011, where he is currently pursuing the Ph.D. degree in electronic engineering. He is a member of the Sensing, Processing and Communication Research Group, Staffordshire University. His current research interests include Internet of Things (IoT), wireless communications, target detection, radar systems, channel estimation techniques, multi antenna systems, and wireless sensor networks.

MOHAMMAD PATWARY (SM'11) received the B.Eng. degree (Hons.) in electrical and electronic engineering from the Chittagong University of Engineering and Technology, Bangladesh, in 1998, and the Ph.D. degree in telecommunication engineering from the University of New South Wales, Sydney, Australia, in 2005. He was with the General Electric Company of Bangladesh from 1998 to 2000 and with Southern-Poro Communications, Sydney Australia, from 2001 to 2002, as a Research and Development Engineer. He was with the University of New South Wales as a Lecturer from 2005 to 2006; then with Staffordshire University, U.K., as a Senior Lecturer from 2006 to 2010; followed by being a Full Professor of wireless systems and digital productivity and the Chair of the Centre of Excellence on Digital Productivity with Connected Services with Staffordshire University untill 2016. He is currently a Full Professor of telecommunication networks and digital productivity and the Head of Research at the Centre for Cloud Computing (CCC), School of Computing and Digital Technologies, Birmingham City University.

His current research interests at CCC include digital productivity with wireless connectivity, sensing and processing for intelligent systems, e.g., manufacturing and healthcare; future network infrastructure, intelligence and QoE measures, wireless communication systems design and optimization, signal processing and energy efficient systems, and future generation of cellular network architecture; and integration of expertise with energy joint source-channel characterization for wireless sensor networks (heterogeneous networks and IoT) and spatial diversity schemes for wireless communications.

ABDEL-HAMID SOLIMAN received the B.Sc. degree in electronic and telecommunications, the M.Sc. degree in smart data acquisition systems, and the Ph.D. degree in image/video processing from Staffordshire University. He has a multi-disciplinary academic/research experience in digital signal processing, telecommunications, data acquisition systems, wireless sensor networks, and image/video processing. In addition to his research activities, he is involved in several enterprise projects and consultancy activities for national and international companies. Now, he is leading and involved in several European funded projects.

MOHAMED ABDEL-MAGUID (SM'11) received the B.Eng. degree (Hons.) in electronics and communications engineering (marine electronics) from AAST, Egypt, in 1992, the M.Sc. degree in telecommunications engineering from AAST, and the Ph.D. degree in electronic engineering from Staffordshire University, U.K. He is currently a Professional Engineer, an Entrepreneur, and a Research and Enterprise focused Academic, with over 25 years of experience in both business and academia. He is currently the founding Chair of the Department of Science and Technology, University of Suffolk, where he is at the forefront of a number of regional STEM skills, research, and innovation agendas in Suffolk. His research spans the areas of telecommunications and intelligent multimodal signal processing and their application to the development of smart systems and intelligent environment. He is particularly interested in next generation networks, cognitive radio, Internet of Things, and data analytics for security, integrated care, and transport applications. He led a portfolio of successful and award winning Applied Research and Business–University collaboration initiatives. His work won the UHNS Clinical Innovation Award in 2010 and the Lord Stafford Award Impact through Innovation in 2009. He held a number of senior positions, both in the U.K. and internationally, and served as a Senior Technology Advisor for government organizations, where he advised on the development of telemedicine initiatives, and the use of smart technologies to improve road safety and technology enhanced learning. He is an Adjunct Professor with the Maastricht School of Management, a fellow of the Chartered Management Institute, and a Co-Opted Member of the BiNDT.